

Zak-OTFS ISAC with Bistatic Sensing via Semi-Blind Atomic Norm Denoising Scheme

Kecheng Zhang, Weijie Yuan, *Senior Member, IEEE*, Maria Sabrina Greco *Fellow, IEEE*

Abstract—Integrated sensing and communication (ISAC) through Zak-transform-based orthogonal time frequency space (Zak-OTFS) modulation is a promising solution for high-mobility scenarios. Realizing accurate bistatic sensing and robust communication necessitates precise channel estimation; however, this remains a formidable challenge in doubly dispersive environments, where fractional delay-Doppler shifts induce severe channel spreading. This paper proposes a semi-blind atomic norm denoising scheme for Zak-OTFS ISAC with bistatic sensing. We first derive the discrete-time input-output (I/O) relationship of Zak-OTFS under fractional delay-Doppler shifts and rectangular windowing. Based on this I/O relation, we formulate the joint channel parameter estimation and data detection task as an atomic norm denoising problem, utilizing the negative square penalty method to handle the non-convex discrete constellation constraints. To solve this problem efficiently, we develop an accelerated iterative algorithm that integrates majorization-minimization, accelerated projected gradient, and inexact accelerated proximal gradient methods. We provide a rigorous convergence proof for the proposed algorithm. Simulation results demonstrate that the proposed scheme achieves super-resolution sensing accuracy and communication performance approaching the perfect channel state information lower bound.

Index Terms—Zak-transform; OTFS; ISAC; Bistatic sensing; Atomic norm denoising.

I. INTRODUCTION

The growing demand for reliable wireless communication in high-mobility scenarios has motivated the search for modulation schemes that operate effectively in doubly dispersive channels [1]. While Orthogonal Frequency Division Multiplexing (OFDM) forms the foundation of 4G and 5G networks [2], [3], it is vulnerable in such rapidly moving environments. The subcarrier orthogonality of OFDM is compromised by high mobility and complex multipath channel environments, resulting in severe inter-carrier interference and performance degradation. Orthogonal Time Frequency Space (OTFS) modulation [4] has emerged as a promising solution to these challenges. By mapping symbols to the delay-Doppler (DD) domain, OTFS leverages the domain’s inherent sparsity and stability to achieve full diversity [5], significantly outperforming OFDM in high-mobility scenarios [4], [5]. Furthermore, because the DD domain directly reflects physical channel parameters, OTFS is inherently suitable for sensing. However, realizing these benefits—whether for robust data detection

Kecheng Zhang and Weijie Yuan are with Guangdong Provincial Key Laboratory of Fully Actuated System Control Theory and Technology, School of Automation and Intelligent Manufacturing, Southern University of Science and Technology, 518055 Shenzhen, China. (email: zhangkc2022@mail.sustech.edu.cn; yuanwj@sustech.edu.cn).

Maria Sabrina Greco is with the Department of Information Engineering, University of Pisa, 56122 Pisa, Italy (e-mail: maria.greco@unipi.it)

or precise sensing—hinges on accurate DD domain channel estimation. In this paper, we consider OTFS-ISAC with bistatic sensing, where the receiver has knowledge of the pilot and frame structure but is unaware of the randomly generated data symbols within the frame. The objective is to detect the transmit data symbols, estimate the DD domain channel parameters, namely channel gains, delays, and Doppler shifts, to simultaneously achieve target sensing and symbol demodulation at the receiver.

A. Literature Review

The realization of OTFS-ISAC with bistatic sensing can be categorized into two classes, which are distinguished primarily by their target parameter estimation methods: two-step ISAC, which first estimates the effective channel matrix and then extracts the parameters from the estimated effective channel, and direct parameter estimation, which directly extracts physical channel parameters from the received DD domain symbols.

1) *Two-Step ISAC*: The two-step ISAC method proceeds by estimating the effective channel matrix as a precursor to identifying the specific channel parameters for target sensing. A representative work on effective channel estimation is [6], where accurate channel estimation is achieved by extracting the DD domain responses of a high-power embedded pilot, where responses exceeding a specific threshold are identified as the effective channel taps. Subsequently, based on the obtained effective channel matrix, spectral estimation methods can be utilized to further extract the DD domain parameters for target sensing [7]. However, this scheme is only applicable to a specific OTFS variant, namely multi-carrier OTFS [8] with ideal pulses. This is because, the ideal pulses satisfy bi-orthogonality [4], which makes the channel response experienced by each symbol depend solely on the transmitting and receiving DD grid indices, independent of the channel parameters (i.e., channel gains, delays, and Doppler shifts). Nevertheless, ideal pulses are physically unrealizable [4]. For physically realizable pulses, such as the rectangular pulse, the channel response, which is jointly determined by both the DD grid indices and the actual channel parameters, varies across symbols [8], [9]. In this case, reconstructing the full DD domain effective channel matrix based solely on the pilot response leads to significant inaccuracies. The simulation results in [8] validate this limitation.

To address the channel estimation challenges associated with multi-carrier OTFS using physically realizable pulses, [8] proposed a novel modulation scheme named Zak-OTFS. This scheme employs the inverse Zak-transform to map signals

from the DD domain to the time domain, and utilizes the Zak-transform to convert the received time-domain signals back to the DD domain. Crucially, the modulation, channel propagation, and demodulation processes can all be formulated via twisted convolution. By leveraging the associative property of twisted convolution, the input-output (I/O) relationship of Zak-OTFS can be equivalently modeled as a twisted convolution between the DD domain effective channel and the transmitted DD symbols. This relationship reveals that every DD domain symbol in Zak-OTFS experiences an identical channel response. Consequently, it becomes feasible to reconstruct the complete effective channel matrix under the practical pulses simply by observing the pilot response. Such a scheme is called ‘model-free’ channel estimation by [8]. Simulation results in [8] demonstrate that with a properly designed frame structure, Zak-OTFS achieves good channel estimation performance with this channel estimation scheme.

However, despite its simplicity, this estimation approach faces a significant challenge. The estimation accuracy is limited by the amount of channel response that can be captured with finite samples. As the spreading of the channel response increases, fewer significant components are sampled, leading to reduced estimation precision. The work [10] analyzed the channel estimation and symbol detection performance of Zak-OTFS under various DD domain pulse shaping filters. It was observed that pulses with lower sidelobes in the ambiguity function yield superior estimation results. Furthermore, if the pulse satisfies the Nyquist ISI criterion, it can also support robust symbol detection. Nevertheless, a fundamental limitation remains due to the infinite nature of the channel response in both the delay and Doppler dimensions, which makes the complete reconstruction of the channel matrix from the finite samples of DD domain pilot responses an intractable problem. Consequently, it will further degrade the accuracy of the subsequent DD domain parameter extraction. In light of this limitation, a viable alternative is to estimate the DD parameters directly.

2) *Parameters Estimation*: For OTFS systems, estimating integer delay and Doppler taps is relatively trivial, achievable by observing the index shifts in the pilot response [11]. In practical ISAC scenarios, it is more common for the delay and Doppler shifts of targets to appear as fractional multiples of the resolutions. The estimation of fractional parameters, however, poses a considerable challenge due to the spread responses.

Existing literature has extensively investigated OTFS channel estimation strategies to cope with fractional delay-Doppler offsets. To address the inter-Doppler interference caused by fractional Doppler shifts, the authors in [12] proposed a cross-correlation-based channel estimation method that utilizes the pilot response in the delay-Doppler domain. The work [13] developed a joint channel estimation and data detection algorithm for LEO satellite communications grounded in the sparse Bayesian learning (SBL) framework. By employing variational Bayesian inference, this method exploits unknown data symbols as virtual pilots to enhance estimation accuracy, demonstrating superior performance over conventional pilot-aided schemes. While the work [13] demonstrated the efficacy of Bayesian inference, it was restricted to integer delay and

Doppler shifts. To address the channel spreading caused by fractional shifts, the work [14] proposed an off-grid SBL scheme that estimates the DD domain channel response. Nevertheless, their specific derivation and analysis primarily assume an OTFS system using ideal pulse shaping, leaving practical waveform scenarios, such as rectangular pulse, less explored. Addressing the limitations of [14], which relied on the bi-orthogonality of ideal pulses to decouple delay and Doppler estimations, the work [15] focused on OTFS systems with practical rectangular waveforms where such decoupling is not possible. They proposed a grid evolution-based SBL scheme that iteratively refines a non-uniform virtual grid to accurately capture the coupled fractional delay and Doppler shifts. While also addressing practical rectangular waveforms and fractional delay-Doppler shifts, the work [16] proposed a DFT-spread OTFS architecture for Terahertz ISAC by utilizing a superimposed pilot scheme and a two-phase estimation algorithm, which sequentially performs coarse integer search followed by off-grid refinement.

While these methods yield good DD domain parameter estimates for enabling OTFS-based target sensing, they face non-trivial limitations. Algorithms based on SBL [14], [15] can estimate the fractional DD domain channel, but their accuracy is intrinsically tied to the grid density, creating a direct trade-off with computational complexity. Similarly, the algorithms proposed in [12], [16] are also constrained by this grid-dependency problem. Crucially, these methods depend on strong assumptions that are often unrealistic in practice; for instance, the integer delay taps assumption in [12] is inappropriate for high-precision ranging, and the assumption of perfect knowledge regarding the number of channel paths in [14]–[16] is idealistic. To the best of our knowledge, there is currently no existing scheme that dispenses with these restrictive assumptions to simultaneously achieve precise channel parameter estimation and symbol detection in doubly dispersive channels. Consequently, developing a robust framework capable of performing these joint tasks is a critical prerequisite for the practical deployment of reliable OTFS-ISAC systems.

B. Contributions

In this paper, we consider performing ISAC with bistatic sensing based on Zak-OTFS. Specifically, our main contributions are summarized as follows:

- *Matrix Form I/O Relation of Zak-OTFS*: Building upon the results in [17], we further derive the discrete-time I/O relationship of Zak-OTFS subject to fractional delay and Doppler shifts and formulate the corresponding matrix-form I/O relation, considering rectangular windowing in both time and frequency domains. We verify that the model-free channel estimation scheme [8] remains applicable to the discrete-time Zak-OTFS. Although, as previously noted, the estimation result through this scheme cannot be used to reconstruct the exact channel, it serves as an excellent initialization for our proposed algorithm.
- *Accelerated Algorithm for ISAC with Bistatic Sensing*: Based on the derived I/O relation, we formulate an atomic

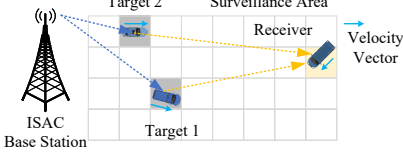


Fig. 1: An illustration of the ISAC scenario.

norm denoising problem and propose an accelerated algorithm capable of simultaneous channel parameter estimation and data symbol detection. Specifically, we employ the negative square penalty method to relax the non-convex discrete constellation constraints on the transmitted symbols into a convex formulation, while leveraging atomic norm denoising to achieve super-resolution estimation of delay and Doppler shifts. During the data symbol update phase, we utilize the accelerated projected gradient (APG) method to perform a single-step iteration on a majorant of the objective function. For the channel vector update, we adopt the inexact accelerated proximal gradient (IAPG) method that optimizes the objective function to ε -optimality. Given that the proposed scheme represents a non-conventional integration of majorization-minimization (MM), APG, and IAPG, we provide a rigorous proof of the algorithm's convergence.

The remainder of this paper is organized as follows. Section II derives the discrete-time I/O relation of Zak-OTFS, which serves as the basis for the atomic norm denoising formulation in Section III. Section IV details the proposed accelerated algorithm and provides a rigorous convergence analysis. Finally, simulation results and conclusions are presented in Sections V and VI, respectively.

Notations: We use x , \mathbf{x} , \mathbf{X} , and \mathcal{X} to represent scalar, column vector, matrix, and set, respectively. The notation $\text{vec}(\cdot)$ represents the vectorization of a matrix by stacking its columns. $\|\cdot\|_2$ denotes the ℓ_2 -norm of a matrix. \mathbb{C} , \mathbb{R} , and \mathbb{Z} denote the sets of complex, real, and integer numbers, respectively; $\langle \mathbf{x}, \mathbf{y} \rangle$ refers to the inner product between two vectors. The superscript $(\cdot)^*$, $(\cdot)^T$ and $(\cdot)^H$ represent the conjugate, the transpose and the conjugate transpose operations, respectively. $\mathbb{I}_{\mathcal{A}}(A)$ denotes an indicator function of \mathcal{A} . \otimes represents the Kronecker product. $A[i, j]$ represents the element in the i -th row and j -th column of matrix \mathbf{A} . \mathbb{N}_n denotes the set $\{0, 1, \dots, n-1\}$.

II. ZAK-OTFS SIGNAL MODEL

This section establishes the Zak-OTFS signal model. We first describe the ISAC scenario considered in this paper and then review the general framework of Zak-OTFS and its OFDM-based implementation. Subsequently, we derive the discrete-time matrix I/O relation and validate the applicability of the model-free channel estimation scheme.

A. General Zak-OTFS I/O Relation

As shown in Fig. 1, in this paper, we consider the scenario where the ISAC base station transmits the Zak-OTFS signal. The surveillance area may contain multiple moving targets.

The transmitted signals illuminate these targets and are subsequently scattered towards the mobile receiver.

For Zak-OTFS [8], we first construct the DD domain transmit signal by summing the multiplications between DD domain transmit symbols and the unfiltered basis functions, $\mathcal{Z}_{p^{\tau_l, \nu_k}}(\tau, \nu)$, i.e.,

$$x_{\text{dd}}(\tau, \nu) = \sum_{l=0}^{M-1} \sum_{k=0}^{N-1} X_{\text{dd}}[l, k] \mathcal{Z}_{p^{\tau_l, \nu_k}}(\tau, \nu), \quad (1)$$

where $X_{\text{dd}}[l, k]$ is the information symbols at DD domain grid (l, k) , $\tau_l = \frac{l}{M\Delta f}$, $\nu_k = \frac{k}{NT}$, T and Δf satisfying $T\Delta f = 1$ are the delay and Doppler periods, respectively and the unfiltered basis function is defined as

$$\mathcal{Z}_{p^{\tau_l, \nu_k}}(\tau, \nu) = \sum_{m \in \mathbb{Z}} \sum_{n \in \mathbb{Z}} e^{j2\pi\nu_k nT} \delta(\tau - \tau_l - nT) \delta(\nu - \nu_k - m\Delta f). \quad (2)$$

By implementing the inverse Zak-transform¹, the corresponding time domain transmit signal is given by

$$x(t) = \sum_{l=0}^{M-1} \sum_{k=0}^{N-1} X_{\text{dd}}[l, k] p^{\tau_l, \nu_k}(t), \quad (3)$$

where $p^{\tau_l, \nu_k}(t)$ is the corresponding time domain unfiltered basis signal,

$$p^{\tau_l, \nu_k}(t) = \sqrt{T} \sum_{n \in \mathbb{Z}} e^{j2\pi\nu_k nT} \delta(t - \tau_l - nT). \quad (4)$$

Since the signal (3) occupies infinite time and frequency domain resources, it is not physically realizable. Both the time and frequency domain resources need to be restricted to implement the Zak-OTFS in practice.

According to [8], [18], we can limit the occupied time and frequency resources by performing a twisted convolution² between a DD domain transmit filter, $g(\tau, \nu)$, and the DD domain transmit signal in (1). The DD domain twisted convolution filtered signal is given by

$$\mathcal{Z}_{x_g}(\tau, \nu) = g *_{\sigma} \mathcal{Z}_x(\tau, \nu), \quad (5)$$

where the corresponding time domain signal is denoted as $x_g(t)$. We obtain the corresponding time domain transmit signal by implementing the inverse Zak-transform on (5). Denoting the doubly-dispersive channel as $h(\tau, \nu)$, the time domain receive signal is

$$r(t) = \iint h(\tau, \nu) x_g(t - \tau) e^{j2\pi\nu(t - \tau)} d\tau d\nu + n(t), \quad (6)$$

where $n(t)$ is the time domain noise. Now we implement Zak-transform³ on (6), the corresponding DD domain receive signal can be represented as [8], [17]

$$\mathcal{Z}_r(\tau, \nu) = h *_{\sigma} \mathcal{Z}_{x_g}(\tau, \nu) = h *_{\sigma} (g *_{\sigma} x_{\text{dd}})(\tau, \nu). \quad (7)$$

¹The inverse Zak-transform is defined as $s(t) \triangleq \sqrt{T} \int_0^{\Delta f} \mathcal{Z}_s(t, \nu) d\nu$, see [8] for more details.

²Consider $a(\tau, \nu)$ and $b(\tau, \nu)$ are function defined on \mathbb{R}^2 , the twisted convolution between them is defined as $a *_{\sigma} b(\tau, \nu) = \iint_{\mathbb{R}^2} a(\tau', \nu') b(\tau - \tau', \nu - \nu') e^{j2\pi\nu'(\tau - \tau')} d\tau' d\nu'$.

³For $T > 0$, the Zak-transform of a continuous time signal $s(t)$ is defined as $\mathcal{Z}_s(\tau, \nu) \triangleq \sqrt{T} \sum_{k=-\infty}^{\infty} s(\tau + kT) e^{-j2\pi k\nu T}$. See [8] for more details.

The receiver side performs another twisted convolution between a DD domain receiving filter, $\tilde{g}(\tau, \nu)$, and the DD domain receive signal (7), and gets the DD domain filtered signal,

$$y_{dd}(\tau, \nu) = \tilde{g} *_{\sigma} \mathcal{Z}_r(\tau, \nu). \quad (8)$$

Put these results together, the DD domain I/O relation of Zak-OTFS is given by

$$y_{dd}(\tau, \nu) = h_{\text{eff}}(\tau, \nu) *_{\sigma} x_{dd}(\tau, \nu) + \tilde{n}_{dd}(\tau, \nu), \quad (9)$$

where $h_{\text{eff}}(\tau, \nu) = \tilde{g} *_{\sigma} h *_{\sigma} g(\tau, \nu)$ is the effective channel response, and $\tilde{n}_{dd}(\tau, \nu) = \tilde{g} *_{\sigma} \mathcal{Z}_n(\tau, \nu)$ is the DD domain effective noise. By sampling $y_{dd}(\tau, \nu)$ at $\tau = \tau_l$ and $\nu = \nu_k$ and omitting the noise term, we have

$$Y_{dd}[l, k] = \sum_{l' \in \mathbb{Z}} \sum_{k' \in \mathbb{Z}} h_{\text{eff}}[l', k'] X_{dd}[l - l', k - k'] e^{j2\pi \frac{k'(l-l')}{MN}}, \quad (10)$$

where $Y_{dd}[l, k]$ is the DD domain received symbols at (l, k) , $h_{\text{eff}}[l, k]$ and $X_{dd}[l, k]$ means sampling $h_{\text{eff}}(\tau, \nu)$ and $x_{dd}(\tau, \nu)$ at $\tau = \tau_l$ and $\nu = \nu_k$, respectively. The equation (10) is called the discrete twisted convolution by [8].

B. Specific Zak-OTFS Implementation via OFDM Framework

In this subsection, we consider a specific implementation of Zak-OTFS and introduce how to realize it under the OFDM framework. First, the DD domain transmit filter is constructed as

$$g(\tau, \nu) = \alpha(\tau)\beta(\nu)e^{j2\pi\tau\nu}. \quad (11)$$

According to [18], performing the twisted convolution with $g(\tau, \nu)$ given in (11) is equivalent to implement frequency domain windowing first and then time domain windowing on (3). The filtered basis function is expressed as

$$p_g^{\tau_l, \nu_k}(t) = \underbrace{B(t)e^{j2\pi\nu_k(t-\tau_l)}}_{\text{Time-limited tone}} \underbrace{\sum_{m \in \mathbb{Z}} A(m\Delta f + \nu_k)e^{j2\pi m\Delta f(t-\tau_l)}}_{\text{Pulse train}}, \quad (12)$$

where $A(f) = \int_{\mathbb{R}} \alpha(\tau)e^{-j2\pi f\tau} d\tau$ is the frequency domain window function, $B(t) = \int_{\mathbb{R}} \beta(\nu)e^{j2\pi\nu t} d\nu$ is the time domain window function, $p_g^{\tau_l, \nu_k}(t)$ is known as *pulsone* [8].

We assume the channel is sparse and there are P resolvable paths, which gives

$$h(\tau, \nu) = \sum_{i=1}^P h_i \delta(\tau - \tau_i) \delta(\nu - \nu_i), \quad (13)$$

where τ_i and ν_i are the delay and Doppler shift of the i -th path, respectively. Then time-domain received signal after passing the channel then becomes

$$r(t) = \sum_{i=1}^P h_i x_g(t - \tau_i) e^{j2\pi\nu_i(t-\tau_i)} + n(t). \quad (14)$$

The DD domain receive filter is constructed as

$$\tilde{g}(\tau, \nu) = \alpha^*(-\tau)\beta^*(-\nu). \quad (15)$$

Performing the twisted convolution between $\tilde{g}(\tau, \nu)$ given in (15) and $r(t)$ is equivalent to time windowing the received

signal $r(t)$ with $B^*(t)$ followed by frequency windowing it with $A^*(f)$.

The transceiver procedure of Zak-OTFS defined in this subsection can be implemented via the OFDM framework, as shown in Fig. 2. We can verify that the DD domain I/O relation under the transceiver frameworks shown in Fig. 2(a) and Fig. 2(b) is exactly the same as (10).

C. Matrix Form I/O Relation of Zak-OTFS

Although the aforementioned continuous-time I/O relation provides mathematical insights, the involved integration operations are computationally prohibitive for practical digital signal processing. To bridge this gap and facilitate computer simulations, we derive a discrete-time counterpart for the Zak-OTFS I/O relationship. As illustrated in Fig. 2b, the receive framework processes the received signal $r(t)$ through three cascading stages: OFDM demodulation, frequency windowing, and postcoding. In the OFDM receiving framework, the received signal is sampled at a rate of $F_s = M\Delta f$. The intermediate vector $\tilde{\mathbf{y}}$ is then obtained by computing the cross-correlation between these signal samples and the discretized basis functions $[B^*(kF_s)e^{-j2\pi \frac{n\Delta f}{N} kF_s}]_{k=0}^{MN-1}$. Then, we perform the subsequent procedures to obtain the DD domain received symbols.

Without loss of generality, we consider that both the time and frequency windows are rectangular functions, i.e., $A(f)$ and $B(t)$ are 1 within the interval $[0, M\Delta f]$ and $[0, NT]$, respectively, and zero, otherwise. Assume the cyclic-prefix (CP) is added in front of the transmit signal $x_g(t)$. After removing the CP at the receiver side, the k -th sample of the time domain received signal is

$$r[k] = \sum_{i=1}^P \sum_{n=0}^{MN-1} h_i s_n e^{j2\pi \left(\frac{n}{NT} + \nu_i\right) \left(\frac{k}{M\Delta f} - \tau_i\right)} + n[k], \quad (16)$$

where s_n is the n -th element of the transmit symbols sequence, \mathbf{s} , given by

$$\mathbf{s} = \text{vec}\{(\mathbf{X}_{dd} \cdot \mathbf{W})^T \mathbf{F}_M\} = (\mathbf{F}_M \otimes \mathbf{I}_N) \widetilde{\mathbf{W}} \mathbf{x}_{dd}, \quad (17)$$

$\mathbf{X}_{dd} \in \mathbb{C}^{M \times N}$ and $\mathbf{x}_{dd} = \text{vec}\{\mathbf{X}_{dd}^T\}$ denote the DD domain symbol matrix and vector, respectively, $\mathbf{W} \in \mathbb{C}^{M \times N}$ is the twiddle factor matrix, $\widetilde{\mathbf{W}} = \text{Diag}\{\text{vec}\{\mathbf{W}^T\}\}$, and $\mathbf{F}_M \in \mathbb{C}^{M \times M}$ is the discrete Fourier transform matrix satisfying $\mathbf{F}_M \mathbf{F}_M^H = \mathbf{I}_M$. Based on (16), the time domain received signal can be rewritten in vector form,

$$\mathbf{r} = \sum_{i=1}^P h_i \mathbf{D}_{\nu_i} \mathbf{F}_{MN}^H \mathbf{B}_{\tau_i} \mathbf{s} + \mathbf{n}, \quad (18)$$

where $\mathbf{B}_{\tau} = \text{Diag}\left\{1, e^{-j2\pi \frac{\tau}{NT}}, \dots, e^{-j2\pi \frac{(MN-1)\tau}{NT}}\right\}$, $\mathbf{D}_{\nu} = \text{Diag}\left\{1, e^{j2\pi \frac{\nu}{M\Delta f}}, \dots, e^{j2\pi \frac{(MN-1)\nu}{M\Delta f}}\right\}$, and $\mathbf{n} \in \mathbb{C}^{MN \times 1}$ is the noise at the receiver side.

Based on the receive framework, the DD domain received signal can also be written in vector form,

$$\mathbf{y}_{dd} = \widetilde{\mathbf{W}} (\mathbf{F}_M^H \otimes \mathbf{I}_N) \mathbf{F}_{MN} \mathbf{r}, \quad (19)$$

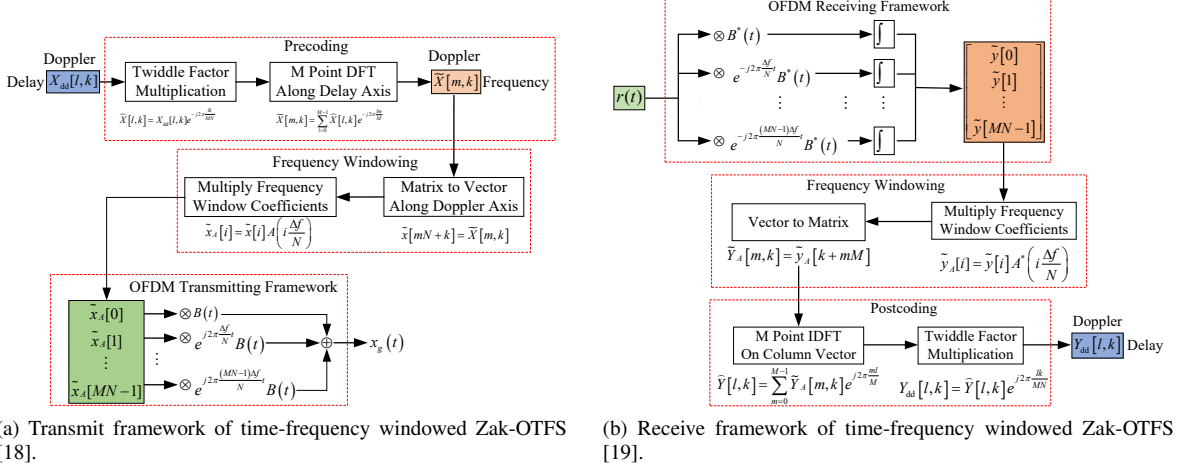


Fig. 2: OFDM-based framework of windowed Zak-OTFS.

$$\sum_{m \in \mathbb{Z}} e^{j2\pi \frac{km}{N}} \mathcal{Y}_A(\tau_{l'} - \tau_l - \tau - mT, -(\nu_{k'} - \nu_k - \bar{m}\Delta f)) \stackrel{(i)}{=} \sum_{m \in \mathbb{Z}} A(\nu_k + m\Delta f) A^*((m - \bar{m})\Delta f + \nu_{k'}) e^{j2\pi \frac{(l' - l - l\tau)(mN + k)}{MN}} \quad (23)$$

where the DD domain receive matrix is obtained by reshaping \mathbf{y}_{dd} back into matrix form by constructing the columns one-by-one, and we denote the procedure as $\mathbf{Y}_{dd} = \text{mat}\{\mathbf{y}_{dd}\}$. The I/O relation (19) can be rewritten as follows

$$\mathbf{y}_{dd} = \mathbf{H}_{\text{eff}} \mathbf{x}_{dd} + \tilde{\mathbf{n}}, \quad (20)$$

where $\tilde{\mathbf{n}} = \widetilde{\mathbf{W}}(\mathbf{F}_M^H \otimes \mathbf{I}_N) \mathbf{F}_{MN} \mathbf{n}$ is the DD domain effective noise vector, and \mathbf{H}_{eff} is the DD domain effective channel matrix given by

$$\mathbf{H}_{\text{eff}} = \widetilde{\mathbf{W}}^H (\mathbf{F}_M^H \otimes \mathbf{I}_N) \mathbf{F}_{MN} \mathbf{H}_{\text{TD}} \mathbf{F}_{MN}^H (\mathbf{F}_M \otimes \mathbf{I}_N) \widetilde{\mathbf{W}}, \quad (21)$$

where $\mathbf{H}_{\text{TD}} = \sum_{i=1}^P h_i \mathbf{D}_{\nu_i} \mathbf{F}_{MN}^H \mathbf{B}_{\tau_i} \mathbf{F}_{MN}$ is the time domain channel matrix. The $(k'M + l', kM + l)$ -th element in \mathbf{H}_{eff} is given by

$$H_{\text{eff}}[k'M + l', kM + l] = \sum_{i=1}^P \sum_{m=0}^{M-1} \sum_{m'=0}^{M-1} h_i e^{j2\pi \frac{l'[k' - k - (m - m')N]}{MN}} \sum_{n=0}^{MN-1} e^{-j2\pi n \frac{k' - k - (m - m')N - k\nu_i}{MN}} e^{j2\pi \frac{(l' - l - l\tau_i)(k + mN)}{MN}}. \quad (22)$$

Noticing that we have the equation in (23), where $\mathcal{Y}_A(\tau, \nu) = \int_{\mathbb{R}} A(f) A^*(f - \nu) e^{j2\pi f \tau} df$ is the ambiguity function of the frequency window [17], and the Poisson summation is applied in (i). Recap that $A(f) = 1$ when $f \in [0, M\Delta f]$, and it is zero, otherwise; together with the fact that $k \in \mathbb{N}_N$ and $k' \in \mathbb{N}_N$, the value of (23) is nonzero only when $m \in \mathbb{N}_M$ and $(m - \bar{m}) \in \mathbb{N}_M$. By denoting $\bar{m} = m - m'$, and substituting (23) into (22), the effective channel matrix can be rewritten as

$$H_{\text{eff}}[k'M + l', kM + l] = \sum_{m \in \mathbb{Z}} \sum_{\bar{m} \in \mathbb{Z}} e^{j2\pi \frac{(k' - k - \bar{m}N)(l + mM)}{MN}} e^{j2\pi \frac{m\bar{k}}{N}} h_{\text{eff}}[l' - l - mM, k' - k - \bar{m}N], \quad (24)$$

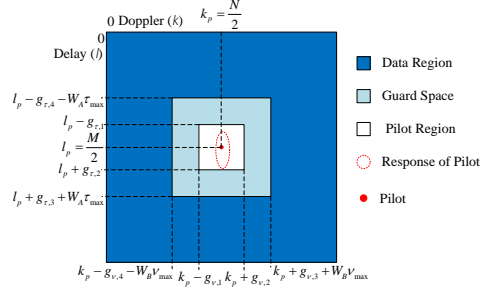


Fig. 3: Zak-OTFS frame with embedded pilot.

where $h_{\text{eff}}[l, k]$ is the effective channel response given by

$$h_{\text{eff}}[l, k] = \sum_{i=1}^P h_i e^{j2\pi \frac{lk}{MN}} \mathcal{Y}_A(\tau_l - \tau_i, -\nu_k) \mathcal{X}_{\tilde{B}}(0, k - k_{\nu_i}), \quad (25)$$

with $\mathcal{X}_{\tilde{B}}(0, k_{\nu}) = \sum_{n=0}^{MN-1} e^{-j2\pi \frac{n k_{\nu}}{MN}}$ being the zero delay-cut on the discrete periodic ambiguity function [20] of the time domain window samples, i.e., $[B(n/F_s)]_{n=0}^{MN-1}$. Combine (20) and (24) together, the element-wise I/O relation for the discretization form of the framework in Fig. 2 can also be expressed as the discretized twisted convolution as in (10) with $h_{\text{eff}}[l, k]$ given in (25), meaning that the model-free channel estimation scheme in [8] still applies in the discrete-time Zak-OTFS.

D. ISAC Scenario and Embedded Pilot Scheme

The Zak-OTFS frame structure with the embedded pilot scheme is shown in Fig. 3. The sizes of guard space and pilot region of the Zak-OTFS frame are determined according to the channel characters, i.e., the maximum delay, τ_{\max} , and the maximum Doppler, ν_{\max} , of the channel. Denoting the pilot

symbol as x_p , which is placed at $(l_p, k_p) = (\lfloor \frac{M}{2} \rfloor, \lfloor \frac{N}{2} \rfloor)$, the received pilot response is

$$y_{dd,p}[l, k] = x_p h_{\text{eff}}[l - l_p, k - k_p] e^{j2\pi \frac{(k-k_p)l_p}{MN}} + \sum_{m \in \mathbb{Z} \setminus \{0\}} \sum_{n \in \mathbb{Z} \setminus \{0\}} x_p h_{\text{eff}}[l - l_p - nM, k - k_p - mN] e^{j2\pi \frac{nk}{N}} e^{j2\pi \frac{(k-k_p-mN)(l_p+nM)}{MN}}. \quad (26)$$

Under the crystalline regime condition [8], which holds when $\tau_{\max} < T$, $\nu_{\max} < \Delta f$, and M and N are large enough, the second term in (26) can be ignored so that the effective channel response can be approximated by sampling the response in pilot region, i.e.,

$$\hat{h}_{\text{eff}}[l, k] = \begin{cases} \frac{y_{dd}[l + l_p, k + k_p]}{x_p} e^{-j2\pi \frac{kl_p}{MN}}, & \text{if } (l, k) \text{ in pilot region,} \\ 0, & \text{otherwise.} \end{cases} \quad (27)$$

The estimated effective channel matrix can be reconstructed through (24) and (27).

III. PROBLEM FORMULATION

In this section, we formulate the optimization problem for Zak-OTFS ISAC. We first formulate the joint estimation task as an atomic norm denoising problem to exploit the sparse nature of the delay-Doppler channel. Subsequently, to address the computational intractability caused by the discrete PSK constellation constraints on information symbols, we introduce a penalty-based reformulation that relaxes the problem into a convex optimization framework, setting the stage for the efficient algorithm developed in the next section.

A. Atomic Norm Formulation

The time-domain I/O relation derived in (18) can be re-expressed in a compact matrix form as follows:

$$\mathbf{r} = (\mathbf{s}^T \otimes \mathbf{I}_{MN}) \text{Diag}\{\text{vec}\{\mathbf{F}_{MN}^H\}\} \mathbf{h} + \mathbf{n}, \quad (28)$$

where the channel vector \mathbf{h} is defined as $\mathbf{h} = \sum_{i=1}^P h_i \mathbf{b}_{\tau_i} \otimes \mathbf{d}_{\nu_i}$, with $\mathbf{b}_{\tau_i} = \text{diag}\{\mathbf{B}_{\tau_i}\}$ and $\mathbf{d}_{\nu_i} = \text{diag}\{\mathbf{D}_{\nu_i}\}$. To leverage the inherent sparsity of the channel in the DD domain, we employ the atomic norm [21] of \mathbf{h} as a regularizer. Consequently, the joint symbol detection and channel estimation task is formulated as an atomic norm denoising problem:

$$\min_{\mathbf{x}_{dd,d}, \mathbf{h}} \frac{1}{2} \|\mathbf{r} - (\mathbf{s}^T \otimes \mathbf{I}_{MN}) \mathbf{D} \mathbf{h}\|_2^2 + \eta \|\mathbf{h}\|_{\mathcal{A}} \quad (29a)$$

$$\text{s.t. } \mathbf{x}_{dd,d} \in \mathcal{S}, \quad (29b)$$

where $\mathbf{x}_{dd,d}$ represents the vector of data information symbols located within the ‘data region’ of the Zak-OTFS frame (which is a sub-vector of \mathbf{x}_{dd}), $\mathbf{D} = \text{Diag}\{\text{vec}\{\mathbf{F}_{MN}^H\}\}$ is a diagonal matrix, and η is the regularization parameter. The set \mathcal{S} denotes the discrete alphabet set (e.g., BPSK or QPSK). The atomic norm $\|\mathbf{h}\|_{\mathcal{A}}$ is defined as [21]:

$$\|\mathbf{h}\|_{\mathcal{A}} = \inf\{t > 0 \mid \mathbf{h} \in t \cdot \text{conv}\{\mathcal{A}\}\}, \quad (30)$$

where \mathcal{A} is the set of atoms [21]:

$$\mathcal{A} = \{e^{j\phi} \mathbf{a}(\tau, \nu) \mid \mathbf{a}(\tau, \nu) = \mathbf{b}_{\tau} \otimes \mathbf{d}_{\nu}, \phi \in [0, 2\pi), (\tau, \nu) \in \Omega\}, \quad (31)$$

and $\text{conv}\{\mathcal{A}\}$ denotes the convex hull of \mathcal{A} .

Directly solving problem (29) presents significant challenges. First, the definition of the atomic norm involves an infinite-dimensional convex hull, which typically requires reformulation into a semi-definite programming (SDP) problem [21]. While methods like the alternating direction method of multipliers (ADMM) can solve such SDPs, they remain computationally expensive for large-scale systems. More critically, the constraint $\mathbf{x}_{dd,d} \in \mathcal{S}$ imposes a discrete, non-convex feasible set, rendering (29) a mixed-integer programming problem that is generally NP-hard. To facilitate efficient gradient-based optimization on processing the constraints on the information symbols, we introduce a penalty-based model that transforms the discrete constraints into an equivalent convex formulation.

B. Penalty-Based Reformulation

To address the intractability of the discrete alphabet constraint, we employ a penalty method that relaxes the discrete set \mathcal{S} to its convex hull while enforcing structure through a negative square penalty term [22], [23]. This strategy transforms the combinatorial problem into a convex optimization problem. Specifically, we relax the constraint $\mathbf{x}_{dd,d} \in \mathcal{S}$ to $\mathbf{x}_{dd,d} \in \bar{\mathcal{S}}$, where $\bar{\mathcal{S}} = \text{conv}\{\mathcal{S}\}$ is the convex hull of the constellation. Ideally, the solution should lie on the vertices of $\bar{\mathcal{S}}$, which correspond to the original discrete symbols. To encourage this, we add a concave penalty term $-\rho \|\mathbf{x}_{dd,d}\|_2^2$ to the objective function [22], [23], resulting in the following formulation:

$$\begin{aligned} \min_{\mathbf{x}_{dd,d}, \mathbf{h}} & \frac{1}{2} \|\mathbf{r} - (\mathbf{s}^T \otimes \mathbf{I}_{MN}) \mathbf{D} \mathbf{h}\|_2^2 - \rho \|\mathbf{x}_{dd,d}\|_2^2 + \eta \|\mathbf{h}\|_{\mathcal{A}} \\ \text{s.t. } & \mathbf{x}_{dd,d} \in \bar{\mathcal{S}}, \end{aligned} \quad (32)$$

where $\rho > 0$ is the penalty parameter. As explained in [23], for constant-modulus constellations (e.g., PSK⁴), the discrete elements of \mathcal{S} are the vertices of $\bar{\mathcal{S}}$ and these vertices maximize the ℓ_2 -norm, $\|\mathbf{x}_{dd,d}\|_2^2$. By promoting a larger norm through the penalty term, the negative square penalty term, i.e., $-\rho \|\mathbf{x}_{dd,d}\|_2^2$, encourages the solution of (32) to approach a discrete constellation point as the penalty weight ρ grows.

This approach is theoretically underpinned by the following lemma, which establishes the equivalence between the relaxed penalty problem and the original discrete problem for sufficiently large penalty parameters.

Lemma 1 [23]. *For any fixed channel vector \mathbf{h} , there exists a threshold $\rho_0 > 0$ such that for all $\rho > \rho_0$, the (local) optimal solution for $\mathbf{x}_{dd,d}$ in the penalty-based problem (32) is identical to that of the original discrete problem (29).*

⁴It is important to note that the penalty method employed here applies only to PSK-modulated symbols. It does not extend to higher-order QAM constellations, such as 16-QAM or above. We consider performing the bistatic ISAC with high-order QAM as our future work.

While penalty methods have been successfully applied to problems like quantized precoding [22]–[24], our current formulation (32) introduces distinct complexities. Unlike prior works that optimize a single variable, our objective function features a bilinear coupling between the optimization variables $\mathbf{x}_{dd,d}$ and \mathbf{h} . This coupling creates a neither convex nor concave objective function with potential saddle points, complicating the convergence analysis. Furthermore, the inclusion of the atomic norm regularizer $\|\mathbf{h}\|_{\mathcal{A}}$ precludes simple gradient-based updates for \mathbf{h} , necessitating sophisticated proximal operations. Addressing these challenges requires a tailored algorithmic framework capable of handling the biconvex structure and the atomic norm regularization efficiently, which we develop in the next section.

IV. ITERATIVE COORDINATE DESCENT METHOD FOR ZAK-OTFS ISAC

In this section, we present an efficient iterative algorithm for joint channel estimation and symbol detection in Zak-OTFS ISAC systems. Then, we provide a theoretical convergence analysis establishing the algorithm's convergence to an ε -stationary point.

A. Our Proposed Algorithm

In this subsection, we propose an iterative algorithm for solving (32). To update the channel vector, we employ an inexact accelerated proximal gradient method to solve the atomic norm denoising subproblem. For the symbol update, we utilize an MM approach solved via accelerated projected gradient descent.

1) *Initialization*: We initialize the algorithm by estimating the channel through (27). By denoting the estimated DD domain channel matrix as $\hat{\mathbf{H}}_{\text{eff}}$, the DD domain transmit symbol vector is detected by LMMSE detector:

$$\hat{\mathbf{x}}_{dd} = \left(\hat{\mathbf{H}}_{\text{eff}}^H \hat{\mathbf{H}}_{\text{eff}} + \sigma^2 \mathbf{I}_{MN} \right)^{-1} \hat{\mathbf{H}}_{\text{eff}}^H \mathbf{y}_{dd}. \quad (33)$$

Then we get the initial channel vector for problem (32) through $\mathbf{h}^{(0)} = \text{vec}\{\mathbf{H}^{(0)}\}$, where $\mathbf{H}^{(0)}$ is given by

$$\mathbf{H}^{(0)} = \mathbf{F}_{MN} \odot \left(\mathbf{Q} \hat{\mathbf{H}}_{\text{eff}} \mathbf{Q}^H \mathbf{F}_{MN}^H \right), \mathbf{Q} = \mathbf{F}_{MN}^H (\mathbf{F}_M \otimes \mathbf{I}_N) \widetilde{\mathbf{W}}.$$

We then obtain the initial time domain signal vector $\mathbf{s}^{(0)}$ through (17) with $\hat{\mathbf{x}}_{dd}$.

2) *Updating the Channel Vector*: Assume the variables have been updated $(t-1)$ times. At the t -th iteration, for the simplicity of notations, we reformulate the subproblem for updating $\mathbf{h}^{(t+1)}$ as below,

$$\min_{\mathbf{h}} \gamma_t(\mathbf{h}) + \eta \|\mathbf{h}\|_{\mathcal{A}}, \quad (34)$$

where $\gamma_t(\mathbf{h}) = \frac{1}{2} \|\mathbf{r} - \mathbf{S}^{(t)} \mathbf{h}\|_2^2$ with $\mathbf{S}^{(t)} = ([\mathbf{s}^{(t)}]^T \otimes \mathbf{I}_{MN}) \mathbf{D}$. Instead of solving problem (34) directly, we consider implementing one-step inexact accelerated proximal-gradient method. Specifically, we choose the Nesterov or FISTA-type acceleration scheme. We update the channel vector by $\mathbf{h}^{(t+1)} = \text{prox}_{\alpha^{(t)}}(\hat{\mathbf{h}}^{(t)})$, where

$$\text{prox}_{\alpha^{(t)}}(\hat{\mathbf{h}}^{(t)}) = \arg \min_{\mathbf{h}} \frac{\alpha^{(t)}}{2} \|\mathbf{h} - \hat{\mathbf{h}}^{(t)}\|_2^2 + \eta \|\mathbf{h}\|_{\mathcal{A}}, \quad (35)$$

$\alpha^{(t)} = \lambda_{\max}([\mathbf{S}^{(t)}]^H \mathbf{S}^{(t)}) = \|\mathbf{s}^{(t)}\|_2^2$ is the maximum eigenvalue, $\hat{\mathbf{h}}^{(t)} = \mathbf{h}^{(t)} - \frac{1}{\alpha^{(t)}} \nabla \gamma_t(\hat{\mathbf{h}}^{(t)})$, $\nabla \gamma_t(\hat{\mathbf{h}}^{(t)})$ is the gradient of $\gamma_t(\mathbf{h})$ at $\hat{\mathbf{h}}^{(t)}$ with

$$\tilde{\mathbf{h}}^{(t)} = \mathbf{h}^{(t)} + \mu^{(t)} (\mathbf{h}^{(t)} - \mathbf{h}^{(t-1)}), \quad (36)$$

and

$$\mu^{(t)} = \frac{\xi^{(t-1)} - 1}{\xi^{(t)}}, \xi^{(t)} = \frac{1 + \sqrt{4[\xi^{(t-1)}]^2}}{2}, \quad (37)$$

and with $\xi^{(-1)} = 0$ and $\mathbf{h}^{(-1)} = \mathbf{h}^{(0)}$.

Solving (34) via the one-step inexact accelerated proximal-gradient method offers two key advantages. First, it ensures numerical stability by preventing oscillation within the solution subspace caused by the rank deficiency of $\mathbf{S}^{(t)}$. Second, it enhances computational efficiency by replacing expensive exact optimization on (34) with a one-step inexact solution towards (35), which suffices for overall convergence. While (35) can be solved via an SDP-based ADMM approach, the computational cost is prohibitive. Instead, we leverage the coordinate descent framework from [25], which exploits the origin-symmetry of the atomic set to achieve an efficiency gain of approximately 10^3 times over state-of-the-art ADMM solver.

Observing that our atomic set \mathcal{A} satisfies this requisite origin-symmetry, we invoke the results from [21], [25] to express the atomic norm (30) in the following equivalent form:

$$\|\mathbf{h}\|_{\mathcal{A}} = \inf_{\substack{(\tau_i, \nu_i) \in \Omega \\ \phi_i \in [0, 2\pi)}} \left\{ \sum_i c_i |\mathbf{h}| = \sum_i c_i e^{j\phi_i} \mathbf{a}(\tau_i, \nu_i), c_i > 0, \mathbf{a}(\tau_i, \nu_i) \in \mathcal{A} \right\}. \quad (38)$$

With (38), problem (29) can be reformulated into a mixed-integer problem

$$\min_{\substack{c_i, \phi_i, L \\ \tau_i, \nu_i, L}} \frac{\alpha^{(t)}}{2} \|\hat{\mathbf{h}}^{(t)} - \sum_{i=1}^L c_i e^{j\phi_i} \mathbf{a}(\tau_i, \nu_i)\|_2^2 + \eta \sum_{i=1}^L c_i. \quad (39)$$

Following the procedure in [25], it can be proved that the two problems (34) and (39) are equivalent. Readers can refer to [25] for the detailed proof. We then implement the framework proposed in [25] for updating the channel vector \mathbf{h} by inexactly solving (39). We summarize the framework in Algorithm 1 for completeness.

As discussed in [26] and the following works performing atomic norm denoising, the regularization parameter on the atomic norm directly balances the error and the sparsity of the solution. Following the derivation procedure in [26, Proposition 1], we set the atomic norm regularization parameter as

$$\eta = \mathbb{E}_{\mathbf{n}} \sup_{\mathbf{a} \in \mathcal{A}} \langle \mathbf{n}, \mathbf{S} \mathbf{a} \rangle = \frac{\sigma \sqrt{MN\pi}}{2} \|\mathbf{s}\|_2^2. \quad (40)$$

In Algorithm 1, it is crucial to reliably solve the problems in step 7 and step 17. Both problems can be treated as conic projections, but due to the nonconvex atomic set \mathcal{A} , these problems are nonconvex. Nevertheless, this projection operation fortunately maintains a separable structure [25].

Algorithm 1 Algorithm for inexactly solving (39)

Require: Gradient step size α ; Result of gradient step $\hat{\mathbf{h}}$; Atomic set \mathcal{A} ; Threshold η ; Tolerance ε ; Maximum iteration K_{\max} .

- 1: Initialize with empty set of tuples \mathcal{U} ; Residual vector $\mathbf{h}_r \leftarrow \hat{\mathbf{h}}$; $L \leftarrow 0$; $i \leftarrow 1$; $\delta \leftarrow \varepsilon/(\alpha\|\hat{\mathbf{h}}\|_2^2/\eta + \varepsilon)$; $\eta' \leftarrow (1 - \delta)\eta$;
- 2: $k \leftarrow 0$;
- 3: **repeat**
- 4: **if** $i \leq L$ **then**
- 5: $(c_i, \mathbf{a}_i) \leftarrow [\mathcal{U}]_i$;
- 6: $\mathbf{h}_r^i \leftarrow \mathbf{h}_r + c_i \mathbf{a}_i$;
- 7: $(c_i, \mathbf{a}_i) \leftarrow \arg \min_{c \in \mathbb{C}, \mathbf{a} \in \mathcal{A}} \frac{\alpha}{2} \|\mathbf{h}_r^i - c\mathbf{a}\|_2^2 + \eta' |c|$;
- 8: $\mathbf{h}_r \leftarrow \mathbf{h}_r^i - c_i \mathbf{a}_i$;
- 9: $[\mathcal{U}]_i \leftarrow (c_i, \mathbf{a}_i)$;
- 10: **if** $c_i == 0$ **then**
- 11: Remove (c_i, \mathbf{a}_i) from \mathcal{U} ;
- 12: $L \leftarrow L - 1$, $i \leftarrow i - 1$;
- 13: **end if**
- 14: $i \leftarrow i + 1$;
- 15: **else if** $\left| \eta \sum_{j=1}^L |c_j| - \langle \mathbf{h}_r, \hat{\mathbf{h}} - \mathbf{h}_r \rangle \right| < \varepsilon$ **then**
- 16: **if** $\sup_{\mathbf{a} \in \mathcal{A}} \langle \mathbf{h}_r, \mathbf{a} \rangle > \eta$ **then**
- 17: $(c_{L+1}, \mathbf{a}_{L+1}) \leftarrow \arg \min_{c \in \mathbb{C}, \mathbf{a} \in \mathcal{A}} \frac{\alpha}{2} \|\mathbf{h}_r - c\mathbf{a}\|_2^2 + \eta' |c|$;
- 18: $\mathbf{h}_r \leftarrow \mathbf{h}_r - c_{L+1} \mathbf{a}_{L+1}$;
- 19: Add $(c_{L+1}, \mathbf{a}_{L+1})$ into \mathcal{U} ;
- 20: $L \leftarrow |\mathcal{U}|$, $i \leftarrow 1$;
- 21: **else**
- 22: Break;
- 23: **end if**
- 24: **else**
- 25: $i \leftarrow 1$;
- 26: **end if**
- 27: $k \leftarrow k + 1$;
- 28: **until** Meet the stop criterion or $k \geq K_{\max}$;

Ensure: \mathcal{U} .

Considering the optimization problem in step 17 and denoting $\tilde{\eta} = \eta'/\alpha$, we have

$$\begin{aligned} \frac{1}{2} \|\mathbf{h}_r - c\mathbf{a}\|_2^2 + \tilde{\eta}|c| &= \frac{1}{2} \left[\|\mathbf{h}_r\|_2^2 \right. \\ &\quad \left. + \left(c\|\mathbf{a}\|_2 + \frac{\tilde{\eta} - \langle \mathbf{h}_r, \mathbf{a} \rangle}{\|\mathbf{a}\|_2} \right)^2 - \frac{(\tilde{\eta} - \langle \mathbf{h}_r, \mathbf{a} \rangle)^2}{\|\mathbf{a}\|_2^2} \right]. \end{aligned} \quad (41)$$

Since the term $\|\mathbf{a}\|_2^2 = (MN)^2$ is irrelevant to the choice of the atom vector \mathbf{a} . The solution to the problem is given as

$$\mathbf{a}^* = \arg \max_{\mathbf{a} \in \mathcal{A}} \langle \mathbf{h}_r, \mathbf{a} \rangle, \quad (42a)$$

$$c^* = \begin{cases} 0, & \langle \mathbf{h}_r, \mathbf{a}^* \rangle \leq \tilde{\eta}, \\ \frac{(\mathbf{h}_r^H \mathbf{a}^*)^*}{(MN)^2} \left(1 - \frac{\tilde{\eta}}{\|\mathbf{h}_r^H \mathbf{a}^*\|} \right), & \langle \mathbf{h}_r, \mathbf{a}^* \rangle > \tilde{\eta}. \end{cases} \quad (42b)$$

Determining \mathbf{a}^* is equivalent to maximizing $|\mathbf{h}_r^H \mathbf{a}|^2$ with respect to τ and ν . However, due to the non-convexity of the objective function and the presence of multiple local extrema, finding the global maximum is non-trivial. Following

the strategy in [25], [27], we adopt a two-stage approach: first, we initialize the parameters by selecting the candidate from an oversampled grid that yields the largest objective value; subsequently, we refine this estimate using the Newton-based gradient ascent method to solve (42a).

3) *Updating the Information Symbols Vector:* Once the channel vector $\mathbf{h}^{(t+1)}$ is updated via Algorithm 1, the subproblem for updating the information symbols $\mathbf{x}_{dd,d}$ in (32) becomes

$$\min_{\mathbf{x} \in \bar{\mathcal{S}}} \phi_{\rho,t}(\mathbf{x}), \quad (43)$$

where $\mathbf{x} = \mathbf{x}_{dd,d}$, $\phi_{\rho,t}(\mathbf{x}) = \frac{1}{2} \|\mathbf{y}_{dd,d}^{(t+1)} - \tilde{\mathbf{H}}^{(t+1)} \mathbf{x}\|_2^2 - \rho \|\mathbf{x}\|_2^2$, $\mathbf{y}_{dd,d}^{(t+1)} = \mathbf{y}_{dd} - \mathbf{H}_{\text{eff}}^{(t+1)} \mathbf{x}_{dd,p}$ represents the DD domain received symbols vector after removing the estimated pilot response with $\mathbf{x}_{dd,p}$ denoting the DD domain pilot vector, $\tilde{\mathbf{H}}^{(t+1)} = \mathbf{H}_{\text{eff}}^{(t+1)}[\text{data indices}]$ is the submatrix by picking the columns of $\mathbf{H}_{\text{eff}}^{(t+1)}$ that corresponds to the position of data symbols in \mathbf{x}_{dd} , $\mathbf{H}_{\text{eff}}^{(t+1)}$ is the DD domain effective channel matrix constructed by the updated channel vector $\mathbf{h}^{(t+1)}$.

We adopt the MM method to solve (43). The update through MM method is to solve the following problem:

$$\min_{\mathbf{x} \in \bar{\mathcal{S}}} \psi_{\rho,t}(\mathbf{x}|\mathbf{x}^{(t)}), \quad (44)$$

where $\psi_{\rho,t}(\mathbf{x}|\mathbf{x}^{(t)})$ is the majorant of $\phi_{\rho,t}(\mathbf{x})$ at $\mathbf{x}^{(t)}$. Specifically, we consider the majorant as

$$\begin{aligned} \psi_{\rho}(\mathbf{x}|\mathbf{x}^{(t)}) &= \frac{1}{2} \|\mathbf{y}_{dd,d}^{(t+1)} - \tilde{\mathbf{H}}^{(t+1)} \mathbf{x}\|_2^2 \\ &\quad - 2\rho \langle \mathbf{x}^{(t)}, \mathbf{x} - \mathbf{x}^{(t)} \rangle - \rho \|\mathbf{x}^{(t)}\|_2^2, \end{aligned} \quad (45)$$

It is easy to verify that $\psi_{\rho,t}(\mathbf{x}|\mathbf{x}^{(t)})$ is a tight upper bound of $\phi_{\rho,t}(\mathbf{x})$ since $\phi_{\rho,t}(\mathbf{x}^{(t)}) = \psi_{\rho,t}(\mathbf{x}^{(t)}|\mathbf{x}^{(t)})$ and $\psi_{\rho,t}(\mathbf{x}|\mathbf{x}^{(t)}) \geq \phi_{\rho,t}(\mathbf{x})$ for any $\mathbf{x} \in \bar{\mathcal{S}}$.

Rather than solving (43) exactly to update \mathbf{x} , we perform one-step accelerated projected-gradient to improve the computation efficiency, i.e., we update $\mathbf{x}^{(t+1)}$ by

$$\mathbf{x}^{(t+1)} = \Pi_{\bar{\mathcal{S}}} \left(\tilde{\mathbf{x}}^{(t)} - \frac{1}{\beta^{(t)}} \nabla \psi_{\rho}(\tilde{\mathbf{x}}^{(t)}|\mathbf{x}^{(t)}) \right), \quad (46)$$

where $\beta^{(t)} = \lambda_{\max}([\tilde{\mathbf{H}}^{(t+1)}]^H \tilde{\mathbf{H}}^{(t+1)})$,

$$\tilde{\mathbf{x}}^{(t)} = \mathbf{x}^{(t)} + \iota^{(t)} (\mathbf{x}^{(t)} - \mathbf{x}^{(t-1)}), \quad (47)$$

with

$$\iota^{(t)} = \frac{\zeta^{(t-1)} - 1}{\zeta^{(t)}}, \quad \zeta^{(t)} = \frac{1 + \sqrt{1 + 4[\zeta^{(t-1)}]^2}}{2}, \quad (48)$$

and with $\zeta^{(-1)} = 0$ and $\mathbf{x}^{(-1)} = \mathbf{x}^{(0)}$. The projection operation in (46) has a closed-form expression, see [22] for details.

Note that obtaining the exact value of ρ_0 in Lemma 1 is difficult in practice. Instead, we use the homotopy technique [28], which starts with a small penalty parameter and increases it gradually, tracking the solution path of the corresponding penalty problems [23]. This procedure eventually identifies a ρ_0 that satisfies Lemma 1. This technique also typically yields much better numerical performance than solving the penalty model (32) directly with an excessively large ρ [22], [23].

Algorithm 2 Algorithm for Bistatic Zak-OTFS ISAC

Require: DD domain received signal \mathbf{y}_{dd} ; Atomic set \mathcal{A} ; Threshold η ; Summable tolerance sequence $\{\varepsilon^{(t)}\}_{t \geq 0}$; Positive integer n ; Penalty parameter upper bound ρ_{upb} ; Maximum iterations T_{max} ; Positive constant $\delta > 0$.

- 1: Initialize according to Section IV-A1;
- 2: $t \leftarrow 0$;
- 3: **repeat**
- 4: Inexactly solve (32) via Algorithm 1 with tolerance $\varepsilon^{(t)}$, and obtain $\mathbf{h}^{(t+1)}$ with $\mathcal{U}^{(t+1)}$;
- 5: Reconstruct the DD domain effective channel with $\mathcal{U}^{(t+1)}$ through (21), and obtain $\mathbf{H}_{eff}^{(t+1)}$;
- 6: Update information symbols sequence $\mathbf{x}_{dd,d}^{(t+1)}$ via (46);
- 7: **if** $\|\mathbf{x}_{dd,d}^{(t+1)} - \mathbf{x}_{dd,d}^{(t)}\|_2^2 \leq \delta$ or $[t]_n = 0$ **then**
- 8: $\rho^{(t+1)} \leftarrow \min\{c\rho^{(t)}, \rho_{upb}\}$;
- 9: **end if**
- 10: Obtain $\mathbf{s}^{(t+1)}$ via (17);
- 11: $t \leftarrow t + 1$;
- 12: **until** $\|\mathbf{h}^{(t+1)} - \mathbf{h}^{(t)}\|_2 \leq \delta$ or t reach maximum iterations T_{max} ;

Ensure: $(\mathbf{h}^{(t)}, \mathbf{x}_{dd,d}^{(t)})$.

B. Convergence Analysis

The procedures for performing Zak-OTFS ISAC is summarized in Algorithm 2. We now analyze its convergence property in this subsection. For the ease of representation, we simplify the notations here. We rewrite the problem (32) as $\min_{\mathbf{x}, \mathbf{h}} F(\mathbf{x}, \mathbf{h})$, where $F(\mathbf{x}, \mathbf{h})$ is given by

$$F(\mathbf{x}, \mathbf{h}) = f(\mathbf{x}, \mathbf{h}) + \mathbb{I}_{\mathcal{S}}(\mathbf{x}), \quad (49)$$

$\mathbf{x} = \mathbf{x}_{dd,d}$, and $f(\mathbf{x}, \mathbf{h})$ is the objective function in (32). We claim the following facts to help the convergence analysis.

1) $\alpha^{(t)} = \|\mathbf{s}^{(t)}\|_2^2$ is bounded by

$$0 < C_s \leq \alpha^{(t)} \leq \bar{C}_s < \infty, \forall t. \quad (50)$$

2) $\beta^{(t)} = \lambda_{\max}([\tilde{\mathbf{H}}^{(t+1)}]^H \tilde{\mathbf{H}}^{(t+1)})$ is bounded by

$$0 < C_h \leq \beta^{(t)} \leq \bar{C}_h < \infty, \forall t. \quad (51)$$

3) $\{\varepsilon^{(t)}\}_{t \geq 0}$ is summable and non-increasing.

With these notations, we now present the convergence result of Algorithm 2 in the following theorem.

Theorem 1. Suppose that $\mu^{(t)}, \nu^{(t)}$ in Algorithm 2 satisfy

$$0 \leq \mu^{(t)} \leq \bar{\mu}, 0 \leq \nu^{(t)} \leq \bar{\nu}, \forall t, \quad (52)$$

where $\bar{\mu} = \sqrt{\frac{C_s}{C_s}(1 - \theta)}$ and $\bar{\nu} = \sqrt{\frac{C_h}{C_h}(1 - \theta)}$ with $0 < \theta \leq 1$. Then, Algorithm 2 will achieve δ away to the ε -stationary point within $\mathcal{O}(1/\delta^2)$ iterations, i.e.,

$$\min_{t'=0,1,\dots,t} \text{dist} \left(\mathbf{0}, \partial_\varepsilon F(\mathbf{x}^{(t'+1)}, \mathbf{h}^{(t'+1)}) \right) \leq \frac{C}{\sqrt{t}}, \quad (53)$$

where the explicit expression of the finite number C is given in Appendix A.

Proof. See Appendix A. □

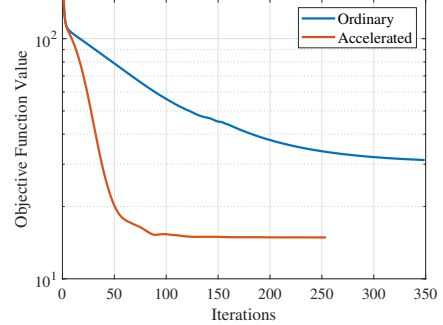


Fig. 4: Iteration performance of the proposed accelerated algorithm and ordinary algorithm.

Although we only proved the algorithm attains an ε -stationary point at a rate of $\mathcal{O}(1/\sqrt{t})$, the derivation provided in Appendix A directly implies a corollary: any limit point of the generated sequence is a stationary point. We omit the proof of this corollary for brevity.

V. NUMERICAL RESULTS

In this section, we evaluate the convergence, communication, and sensing performance of the proposed algorithm. We adopt the Zak-OTFS frame structure shown in Fig. 3 with dimensions $M = 8$ and $N = 16$. Without loss of generality, we assume that the scenario contains at least one target and that no line-of-sight (LoS) link exists between the ISAC base station and the receiver. This assumption facilitates the analysis of the target detection and parameter estimation performance of the proposed algorithm. The system operates at the carrier frequency of 24 GHz with the subcarrier spacing being $\Delta f = 30$ kHz. The pilot is positioned at grid (4, 8), enclosed by a pilot region $[2, 6] \times [5, 11]$ and a guard space $[1, 7] \times [4, 12]$. Data symbols have unit magnitude, while the pilot magnitude is set to $\sqrt{63}$ to normalize the total transmit power to MN . The simulation assumes a bistatic ISAC scenario with up to two targets. The first target has zero delay, while the second target's delay is uniformly distributed in $[0.5, 1.5]/(M\Delta f)$. Doppler shifts are independently drawn from $[0, 1.5]/(NT)$, and channel gains follow a $\mathcal{CN}(0, 1)$ distribution⁵. The receiver only has the knowledge of the Zak-OTFS frame structure and the pilot configuration, the data symbols embedded within the frame are randomly generated and remain unknown. To ensure the reliability of the simulation results, we conducted 5000 Monte Carlo simulations. In each simulation, the channel information and the information symbols within the frame were randomly generated.

A. Convergence Performance of Proposed Algorithm

Fig. 4 illustrates the convergence behavior of the objective function value in (29). The ‘Ordinary’ baseline, representing

⁵Although realistic moving targets exhibit Radar Cross Section (RCS) fluctuations (typically characterized by Swerling models), we adopt this simplified model to align with prevalent ISAC studies. Note that our framework is generic and can be extended to fluctuating scenarios by incorporating the corresponding amplitude statistics into the threshold (40).

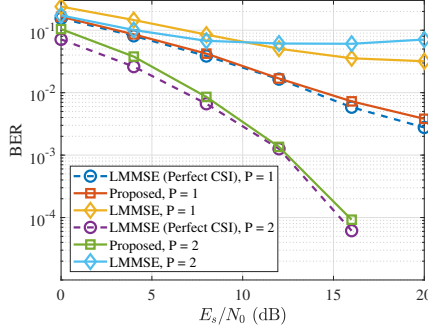


Fig. 5: BER performance with BPSK modulation.

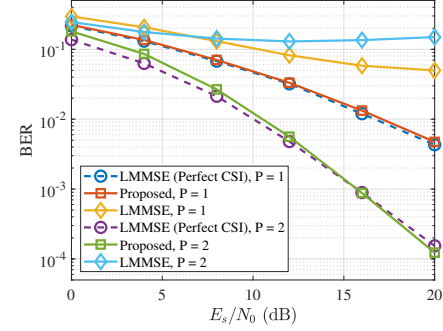


Fig. 6: BER performance with QPSK modulation.

the scheme without extrapolation steps ($\mu^{(t)} = \iota^{(t)} = 0$), exhibits a strictly monotonic but slow descent, failing to reach the error floor even after 350 iterations. In sharp contrast, the proposed ‘Accelerated’ algorithm demonstrates a much faster descent in the objective value, converging to a stable value within merely 150 iterations. Although the accelerated curve is not a strict descent method, it achieves a significantly faster convergence rate and superior computational efficiency compared to the ordinary scheme.

B. Communication Performance

Fig. 5 and Fig. 6 evaluate the Bit Error Rate (BER) performance of the proposed algorithm under BPSK and QPSK modulations, respectively. As benchmarks, we compare against an ‘LMMSE (Perfect CSI)’ lower bound, which assumes perfect knowledge of the effective channel matrix in (20), and a standard ‘LMMSE’ scheme detecting the symbols with the estimated channel by the model-free scheme in (27). The results demonstrate that the proposed algorithm significantly outperforms the standard LMMSE approach, the BERs of the proposed algorithm closely approach the perfect CSI lower bound across the entire SNR range. This superior performance stems from the precise channel estimation provided by the atomic norm denoising scheme. The performance gap between the proposed method and the perfect CSI bound is attributed to channel estimation errors caused by noise. The slightly larger gap under $P = 2$ targets scenario is caused by the interference between pilot responses. Furthermore, the BERs are lower in the $P = 2$ case compared to the $P = 1$ case under both the BPSK and QPSK modulation, which confirms that the proposed algorithm effectively exploits the delay-Doppler diversity of OTFS [29], yielding superior error performance as the number of resolvable paths increases.

C. Sensing Performance

The sensing performance is evaluated using the same Monte-Carlo samples as the communication performance evaluation. To evaluate multi-target performance, we perform optimal data association between the ground truths and estimates using the Hungarian algorithm [30] based on the absolute error of the delay-Doppler pairs. A valid detection is declared only if the matched estimate falls within a predefined distance

(half of resolution in our simulation). Otherwise, it will be considered as a false alarm. The probability of detection is calculated as the ratio of these valid matches to the total number of ground truth targets. It is worth noting that in our simulations, we assume the persistent presence of a target, i.e., there exists at least one propagation path from the ISAC base station to the receiver. Consequently, the resulting detection rate and false alarm rate differ from the standard definitions in classical radar signal processing. As illustrated in Fig. 7?? and Fig. 8??, the target detection performance is consistent across both BPSK and QPSK modulation schemes. For single-target scenarios, the proposed algorithm maintains a high detection probability even at low SNRs, accompanied by an increased false alarm rate. In contrast, detection performance degrades significantly in the two-target scenario at low SNRs. This decline is attributed to mutual interference between target responses; specifically, in high-noise environments, the reflection from a weaker target can be easily masked by the noise floor together with the sidelobes of the stronger target’s response.

The Root Mean Square Error (RMSE) performance for range, velocity, and channel estimation under BPSK and QPSK modulations is illustrated in Figs. 7??-?? and Figs. 8??-??, respectively. It is observed that the parameter estimation RMSE reduces more rapidly with respect to SNR in the single-target case compared to the two-target scenario. This disparity arises because the overlapped channel responses in the multi-target scenario create mutual interference, which hinders precise parameter resolution. Consequently, the overall channel estimation RMSE is consistently higher for the $P = 2$ case across both modulation schemes.

VI. CONCLUSION

In this paper, we proposed an accelerated algorithm for bistatic ISAC within the Zak-OTFS framework. Addressing a scenario where only the pilot and frame structure are known at the receiver, the proposed method achieves simultaneous channel parameter estimation and information symbol detection. Specifically, the algorithm is initialized via model-free channel estimation and LMMSE detection, followed by an iterative process that employs an inexact accelerated proximal gradient step for channel updates and an accelerated projected gradient step for symbol refinement. Simulation results validate

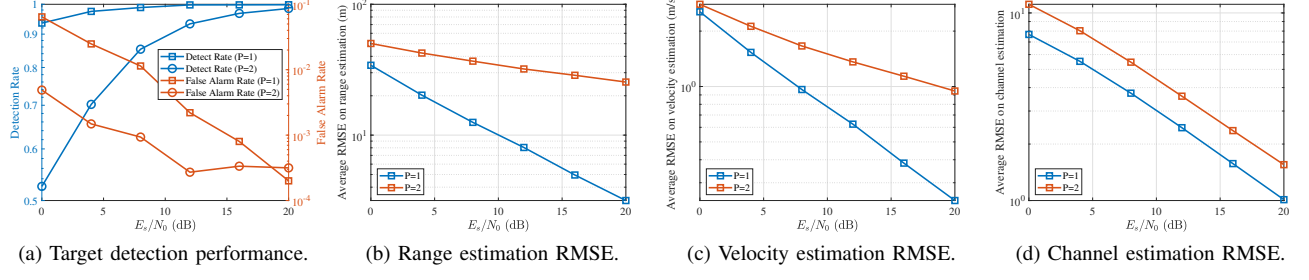


Fig. 7: Sensing performance with BPSK modulation.

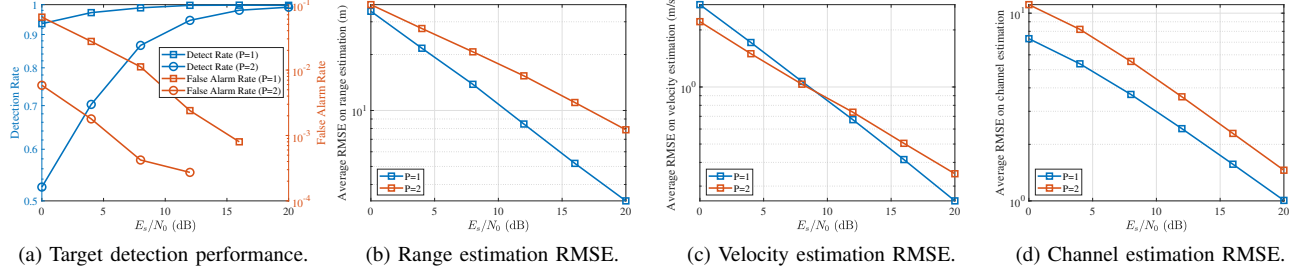


Fig. 8: Sensing performance with QPSK modulation.

the robust convergence of the algorithm and demonstrate its superiority in both sensing and communication performance.

APPENDIX A PROOF OF THEOREM 1

The proof establishes the convergence of Algorithm 2 by demonstrating that the objective function decreases sufficiently across iterations and subsequently confirming that the algorithm converges to an ε -stationary point. We first leverage the properties of the inexact accelerated proximal gradient update for the channel vector and the accelerated projected gradient update for the symbol vector to derive a descent inequality. By summing these descent terms and exploiting the lower-boundedness of the objective function, we establish an $\mathcal{O}(1/\sqrt{t})$ convergence rate to the set of ε -stationary points. The following lemma is useful to the proof.

Lemma 2 [31]. *If $\mathbf{h}^{(t+1)}$ is an $\varepsilon^{(t)}$ -optimal solution to the proximal problem (35), then there exists a vector $\boldsymbol{\delta}^{(t)}$ such that $\|\boldsymbol{\delta}^{(t)}\|_2 \leq \sqrt{\frac{2\varepsilon^{(t)}}{\alpha^{(t)}}}$ and*

$$\alpha^{(t)}[\tilde{\mathbf{h}}^{(t)} - \mathbf{h}^{(t+1)} - \frac{1}{\alpha^{(t)}}\nabla\gamma_t(\tilde{\mathbf{h}}^{(t)}) - \boldsymbol{\delta}^{(t)}] \in \partial_{\varepsilon^{(t)}}\varphi(\mathbf{h}^{(t+1)}), \quad (54)$$

where $\partial_{\varepsilon^{(t)}}\varphi(\mathbf{h}^{(t+1)})$ is the $\varepsilon^{(t)}$ -subgradient of $\varphi(\mathbf{h})$ at $\mathbf{h}^{(t+1)}$ [32, Section 4.3].

A. Upper Boundness of Approximate Stationarity

The update rule of (46) is equivalent to

$$\mathbf{x}^{(t+1)} = \arg \min_{\mathbf{x}} \frac{\beta^{(t)}}{2} \|\mathbf{x} - \tilde{\mathbf{x}}^{(t)}\|_2^2 + \mathbb{I}_{\mathcal{S}}(\mathbf{x}), \quad (55)$$

where $\tilde{\mathbf{x}}^{(t)} = \tilde{\mathbf{x}}^{(t)} - \frac{1}{\beta^{(t)}}\nabla\psi(\tilde{\mathbf{x}}^{(t)}|\mathbf{x}^{(t)})$. According to the first-order optimality, it gives

$$\mathbf{0} \in \beta^{(t)}(\mathbf{x}^{(t+1)} - \tilde{\mathbf{x}}^{(t)}) + \nabla\psi(\tilde{\mathbf{x}}^{(t)}|\mathbf{x}^{(t)}) + \partial\mathbb{I}_{\mathcal{S}}(\mathbf{x}^{(t+1)}). \quad (56)$$

Moreover, since $\mathbf{h}^{(t+1)}$ is an $\varepsilon^{(t)}$ -optimal solution to the proximal problem (35), according to Lemma 2, we have

$$\mathbf{0} \in \alpha^{(t)}(\mathbf{h}^{(t+1)} - \tilde{\mathbf{h}}^{(t)} + \boldsymbol{\delta}^{(t)}) + \nabla\gamma_t(\tilde{\mathbf{h}}^{(t)}) + \partial_{\varepsilon^{(t)}}\psi(\mathbf{h}^{(t+1)}). \quad (57)$$

By denoting $\mathbf{e}_x^{(t+1)} = \nabla\phi_{\rho,t}(\mathbf{x}^{(t+1)}) + \mathbf{v}_x^{(t+1)}$ and $\mathbf{e}_h^{(t+1)} = \nabla\gamma_{t+1}(\mathbf{h}^{(t+1)}) + \mathbf{v}_{h,\varepsilon^{(t)}}^{(t+1)}$ with $\mathbf{v}_x^{(t+1)} \in \partial\mathbb{I}_{\mathcal{S}}(\mathbf{x}^{(t+1)})$ and $\mathbf{v}_{h,\varepsilon^{(t)}}^{(t+1)} \in \partial_{\varepsilon^{(t)}}\psi(\mathbf{h}^{(t+1)})$ being such that

$$\begin{aligned} \mathbf{0} &= \beta^{(t)}(\mathbf{x}^{(t+1)} - \tilde{\mathbf{x}}^{(t)}) + \nabla\psi(\tilde{\mathbf{x}}^{(t)}|\mathbf{x}^{(t)}) + \mathbf{v}_x^{(t+1)}, \\ \mathbf{0} &= \alpha^{(t)}(\mathbf{h}^{(t+1)} - \tilde{\mathbf{h}}^{(t)} + \boldsymbol{\delta}^{(t)}) + \nabla\gamma_t(\tilde{\mathbf{h}}^{(t)}) + \mathbf{v}_{h,\varepsilon^{(t)}}^{(t+1)}, \end{aligned} \quad (58)$$

we then have

$$\begin{aligned} \mathbf{e}_x^{(t+1)} &\in \partial_{\mathbf{x}}F(\mathbf{x}^{(t+1)}, \mathbf{h}^{(t+1)}), \\ \mathbf{e}_h^{(t+1)} &\in \partial_{\mathbf{h},\varepsilon^{(t)}}F(\mathbf{x}^{(t+1)}, \mathbf{h}^{(t+1)}), \end{aligned} \quad (59)$$

where $\partial_{\mathbf{x}}F(\mathbf{x}^{(t+1)}, \mathbf{h}^{(t+1)})$ is the subgradient of $F(\mathbf{x}, \mathbf{h}^{(t+1)})$ towards $\mathbf{x}^{(t+1)}$ and $\partial_{\mathbf{h},\varepsilon^{(t)}}F(\mathbf{x}^{(t+1)}, \mathbf{h}^{(t+1)})$ represents the $\varepsilon^{(t)}$ -subgradient of $F(\mathbf{x}^{(t+1)}, \mathbf{h})$ at $\mathbf{h}^{(t+1)}$. Recap the properties about ε -subgradient in [32],

$$\begin{aligned} \cap\partial_{\varepsilon\downarrow 0}\psi(\mathbf{h}) &= \partial\psi(\mathbf{h}), \\ \partial_{\varepsilon^{(1)}}(\mathbf{h}) &\subset \partial_{\varepsilon^{(2)}}(\mathbf{h}), \text{ if } 0 < \varepsilon^{(1)} < \varepsilon^{(2)}, \end{aligned}$$

we then have

$$\partial_{\mathbf{x}}F(\mathbf{x}^{(t+1)}, \mathbf{h}^{(t+1)}) \subset \partial_{\mathbf{x},\varepsilon^{(t)}}F(\mathbf{x}^{(t+1)}, \mathbf{h}^{(t+1)}), \quad (60)$$

where $\partial_{\mathbf{x}, \varepsilon^{(t)}} F(\mathbf{x}^{(t+1)}, \mathbf{h}^{(t+1)})$ is the corresponding $\varepsilon^{(t)}$ -subgradient. Now, we get

$$\begin{aligned} & \|\mathbf{e}_{\mathbf{x}}^{(t+1)}\|_2 \\ &= \|\nabla \phi_{\rho, t}(\mathbf{x}^{(t+1)}) - \nabla \psi_{\rho, t}(\tilde{\mathbf{x}}^{(t)}|\mathbf{x}^{(t)}) - \beta^{(t)}(\mathbf{x}^{(t+1)} - \tilde{\mathbf{x}}^{(t)})\|_2 \\ &\leq \|\nabla \phi_{\rho, t}(\mathbf{x}^{(t+1)}) - \nabla \psi_{\rho, t}(\tilde{\mathbf{x}}^{(t)}|\mathbf{x}^{(t)})\|_2 + \beta^{(t)}\|\mathbf{x}^{(t+1)} - \tilde{\mathbf{x}}^{(t)}\|_2. \end{aligned} \quad (61)$$

The first term of (61) can be upper bounded by

$$\begin{aligned} & \|\nabla \phi_{\rho, t}(\mathbf{x}^{(t+1)}) - \nabla \psi_{\rho, t}(\tilde{\mathbf{x}}^{(t)}|\mathbf{x}^{(t)})\|_2 \\ &\leq \|\nabla \phi_{\rho, t}(\mathbf{x}^{(t+1)}) - \nabla \phi_{\rho, t}(\mathbf{x}^{(t)})\|_2 \\ &\quad + \|\nabla \psi_{\rho, t}(\mathbf{x}^{(t)}|\mathbf{x}^{(t)}) - \nabla \psi_{\rho, t}(\tilde{\mathbf{x}}^{(t)}|\mathbf{x}^{(t)})\|_2 \\ &\leq (\sqrt{\beta^{(t)}} + 2\rho)\|\mathbf{x}^{(t+1)} - \mathbf{x}^{(t)}\|_2 + \sqrt{\beta^{(t)}\iota^{(t)}}\|\mathbf{x}^{(t)} - \mathbf{x}^{(t-1)}\|_2. \end{aligned} \quad (62)$$

The second term of (61) can be upper bounded by

$$\begin{aligned} & \beta^{(t)}\|\mathbf{x}^{(t+1)} - \tilde{\mathbf{x}}^{(t)}\|_2 \\ &\leq \beta^{(t)}\|\mathbf{x}^{(t+1)} - \mathbf{x}^{(t)}\|_2 + \beta^{(t)}\iota^{(t)}\|\mathbf{x}^{(t)} - \mathbf{x}^{(t-1)}\|_2. \end{aligned} \quad (63)$$

Combining the results in (62) and (63), we have

$$\|\mathbf{e}_{\mathbf{x}}^{(t+1)}\|_2 \leq C_x^{(t)}(\|\mathbf{x}^{(t+1)} - \mathbf{x}^{(t)}\|_2 + \|\mathbf{x}^{(t)} - \mathbf{x}^{(t-1)}\|_2), \quad (64)$$

where $C_x^{(t)} = 2\rho + (1 + \iota^{(t)})(\beta^{(t)} + \sqrt{\beta^{(t)}})$ is finite for all t .

Similarly, we can bound $\|\mathbf{e}_{\mathbf{h}}^{(t+1)}\|_2$ by

$$\begin{aligned} & \|\mathbf{e}_{\mathbf{h}}^{(t+1)}\|_2 \\ &= \|\nabla \gamma_{t+1}(\mathbf{h}^{(t+1)}) - \alpha^{(t)}(\mathbf{h}^{(t+1)} - \tilde{\mathbf{h}}^{(t)} + \delta^{(t)}) - \nabla \gamma_t(\tilde{\mathbf{h}}^{(t)})\|_2 \\ &\leq \|\nabla \gamma_{t+1}(\mathbf{h}^{(t+1)}) - \nabla \gamma_t(\tilde{\mathbf{h}}^{(t)})\|_2 + \alpha^{(t)}\|\mathbf{h}^{(t+1)} - \tilde{\mathbf{h}}^{(t)}\|_2 \\ &\quad + \sqrt{2\alpha^{(t)}\varepsilon^{(t)}}. \end{aligned} \quad (65)$$

The first term of (65) can be upper bounded by

$$\begin{aligned} & \|\nabla \gamma_{t+1}(\mathbf{h}^{(t+1)}) - \nabla \gamma_t(\tilde{\mathbf{h}}^{(t)})\|_2 \\ &\leq \|(\mathbf{S}^{(t+1)} + \mathbf{S}^{(t)})^H \mathbf{h}^{(t+1)}\|_2 + \|\mathbf{r}\|_2\|\mathbf{S}^{(t+1)} - \mathbf{S}^{(t)}\|_2 \\ &\quad + \sqrt{\alpha^{(t)}}\|\mathbf{h}^{(t+1)} - \mathbf{h}^{(t)}\|_2 + \mu^{(t)}\sqrt{\alpha^{(t)}}\|\mathbf{h}^{(t)} - \mathbf{h}^{(t-1)}\|_2. \end{aligned} \quad (66)$$

The second term of (65) can be upper bounded by

$$\begin{aligned} & \alpha^{(t)}\|\mathbf{h}^{(t+1)} - \tilde{\mathbf{h}}^{(t)}\|_2 \\ &\leq \alpha^{(t)}\|\mathbf{h}^{(t+1)} - \mathbf{h}^{(t)}\|_2 + \alpha^{(t)}\mu^{(t)}\|\mathbf{h}^{(t)} - \mathbf{h}^{(t-1)}\|_2. \end{aligned} \quad (67)$$

Since $\|\mathbf{S}^{(t+1)} - \mathbf{S}^{(t)}\|_2 = \|\mathbf{x}^{(t+1)} - \mathbf{x}^{(t)}\|_2$ according to (17), we get

$$\begin{aligned} \|\mathbf{e}_{\mathbf{h}}^{(t+1)}\|_2 &\leq C_h^{(t)}(\|\mathbf{h}^{(t+1)} - \mathbf{h}^{(t)}\|_2 + \|\mathbf{h}^{(t)} - \mathbf{h}^{(t-1)}\|_2) \\ &\quad + C_s^{(t)}\|\mathbf{x}^{(t+1)} - \mathbf{x}^{(t)}\|_2 + \sqrt{2\alpha^{(t)}\varepsilon^{(t)}}, \end{aligned} \quad (68)$$

where both $C_h^{(t)} = (\alpha^{(t)} + \sqrt{\alpha^{(t)}})(1 + \mu^{(t)})$ and $C_s^{(t)} = \|(\mathbf{S}^{(t+1)} + \mathbf{S}^{(t)})^H \mathbf{h}^{(t+1)}\|_2 + \|\mathbf{r}\|_2$ are finite.

Therefore, the distance between $\mathbf{0}$ and the $\varepsilon^{(t)}$ -subgradient of $F(\mathbf{x}, \mathbf{h})$ at $(\mathbf{x}^{(t+1)}, \mathbf{h}^{(t+1)})$ is upper bounded by

$$\begin{aligned} & \text{dist}(\mathbf{0}, \partial_{\varepsilon^{(t)}} F(\mathbf{x}^{(t+1)}, \mathbf{h}^{(t+1)})) \\ &\leq \bar{C}(\|\mathbf{x}^{(t+1)} - \mathbf{x}^{(t)}\|_2 + \|\mathbf{x}^{(t)} - \mathbf{x}^{(t-1)}\|_2 + \|\mathbf{h}^{(t+1)} - \mathbf{h}^{(t)}\|_2 \\ &\quad + \|\mathbf{h}^{(t)} - \mathbf{h}^{(t-1)}\|_2) + \sqrt{2\alpha^{(t)}\varepsilon^{(t)}}, \end{aligned} \quad (69)$$

where $\bar{C} = \sup_t \{C_h^{(t)}, C_s^{(t)}, C_x^{(t)}\}$ is finite.

B. Upper Boundness of Descents

1) *Upper Boundness of $f(\mathbf{x}^{(t)}, \mathbf{h}^{(t+1)}) - f(\mathbf{x}^{(t)}, \mathbf{h}^{(t)})$:* Since Algorithm 1 solves (39) into $\varepsilon^{(t)}$ -optimally, we then have

$$f(\mathbf{x}^{(t)}, \mathbf{h}^{(t+1)}) \leq \varepsilon^{(t)} + \inf_{\mathbf{h}} \{f(\mathbf{x}^{(t)}, \mathbf{h})\}. \quad (70)$$

According to the result in [25], Algorithm 1 arrives (70) within finite iterations. Since $\gamma_t(\mathbf{h})$ in (34) is convex and $\alpha^{(t)}$ -Lipschitz, $\gamma_t(\mathbf{h}^{(t+1)})$ can be bounded as follows:

$$\begin{aligned} & \gamma_t(\mathbf{h}^{(t+1)}) \\ &\leq \gamma_t(\tilde{\mathbf{h}}^{(t)}) + \langle \nabla \gamma_t(\tilde{\mathbf{h}}^{(t)}), \mathbf{h}^{(t+1)} - \tilde{\mathbf{h}}^{(t)} \rangle + \frac{\alpha^{(t)}}{2}\|\mathbf{h}^{(t+1)} - \tilde{\mathbf{h}}^{(t)}\|_2^2 \\ &\leq \gamma_t(\mathbf{h}^{(t)}) + \langle \nabla \gamma_t(\tilde{\mathbf{h}}^{(t)}), \tilde{\mathbf{h}}^{(t)} - \mathbf{h}^{(t)} \rangle + \langle \nabla \gamma_t(\tilde{\mathbf{h}}^{(t)}), \mathbf{h}^{(t+1)} - \tilde{\mathbf{h}}^{(t)} \rangle \\ &\quad + \frac{\alpha^{(t)}}{2}\|\mathbf{h}^{(t+1)} - \tilde{\mathbf{h}}^{(t)}\|_2^2. \end{aligned} \quad (71)$$

Since $\mathbf{h}^{(t+1)}$ is an $\varepsilon^{(t)}$ -optimal solution of (35), according to Lemma 2, we have

$$\begin{aligned} \varphi(\mathbf{h}^{(t+1)}) &\leq \varphi(\mathbf{h}^{(t)}) - \langle \nabla \gamma_t(\tilde{\mathbf{h}}^{(t)}), \mathbf{h}^{(t+1)} - \mathbf{h}^{(t)} \rangle \\ &\quad + \alpha^{(t)}(\delta^{(t)} + \mathbf{h}^{(t+1)} - \tilde{\mathbf{h}}^{(t)}, \mathbf{h}^{(t+1)} - \mathbf{h}^{(t)}) + \varepsilon^{(t)}. \end{aligned} \quad (72)$$

By adding (71) and (72) together and substituting $\tilde{\mathbf{h}}^{(t)}$ in (36) into the result, after some calculations, it gives:

$$\begin{aligned} & f(\mathbf{x}^{(t)}, \mathbf{h}^{(t+1)}) - f(\mathbf{x}^{(t)}, \mathbf{h}^{(t)}) \leq \sqrt{2\alpha^{(t)}\varepsilon^{(t)}}\|\mathbf{h}^{(t+1)} - \mathbf{h}^{(t)}\|_2 \\ &\quad - \frac{\alpha^{(t)}}{2} \left(\|\mathbf{h}^{(t+1)} - \mathbf{h}^{(t)}\|_2^2 - \bar{\mu}^2\|\mathbf{h}^{(t)} - \mathbf{h}^{(t-1)}\|_2^2 \right) + \varepsilon^{(t)}, \end{aligned} \quad (73)$$

where $\|\delta^{(t)}\|_2 \leq \sqrt{\frac{2\varepsilon^{(t)}}{\alpha^{(t)}}}$ is implemented with Cauchy-Schwartz inequality to further upperbound the result.

2) *Upper Boundness of $f(\mathbf{x}^{(t+1)}, \mathbf{h}^{(t+1)}) - f(\mathbf{x}^{(t)}, \mathbf{h}^{(t+1)})$:* The following lemma is useful to derive the upper boundness.

Lemma 3 [33]. *Let*

$$\mathbf{x}^+ = \Pi_{\mathcal{X}} \left(\mathbf{z} - \frac{1}{\beta} \nabla H(\mathbf{z}) \right), \quad (74)$$

where $\mathbf{z} = \mathbf{x} + \alpha(\mathbf{x} - \bar{\mathbf{x}})$ with $\mathbf{x}, \bar{\mathbf{x}} \in \mathcal{X}$, $\alpha \geq 0$; H is convex and has Lipschitz continuous gradient; \mathcal{X} is convex; β is chosen to satisfy

$$H(\mathbf{x}^+) \leq H(\mathbf{z}) + \langle \nabla H(\mathbf{z}), \mathbf{x}^+ - \mathbf{z} \rangle + \frac{\beta}{2}\|\mathbf{x}^+ - \mathbf{z}\|_2^2. \quad (75)$$

Then, it holds that

$$H(\mathbf{x}) - H(\mathbf{x}^+) \geq \frac{\beta}{2}(\|\mathbf{x}^+ - \mathbf{x}\|_2^2 - \alpha^2\|\mathbf{x} - \bar{\mathbf{x}}\|_2^2). \quad (76)$$

According to the update rule (46) and Lemma 3, we have

$$\begin{aligned} & f(\mathbf{x}^{(t+1)}, \mathbf{h}^{(t+1)}) - f(\mathbf{x}^{(t)}, \mathbf{h}^{(t+1)}) \\ &\leq \psi_{\rho, t}(\mathbf{x}^{(t+1)}|\mathbf{x}^{(t)}) - \psi_{\rho, t}(\mathbf{x}^{(t)}|\mathbf{x}^{(t)}) \\ &\leq -\frac{\beta^{(t)}}{2}(\|\mathbf{x}^{(t+1)} - \mathbf{x}^{(t)}\|_2^2 - \bar{\mu}^2\|\mathbf{x}^{(t)} - \mathbf{x}^{(t-1)}\|_2^2). \end{aligned} \quad (77)$$

$$\begin{aligned}
\sum_{t'=0}^t \frac{\alpha^{(t')}}{2} \left(\|\mathbf{h}^{(t'+1)} - \mathbf{h}^{(t')}\|_2^2 - \bar{\mu}^2 \|\mathbf{h}^{(t')} - \mathbf{h}^{(t'-1)}\|_2^2 \right) &= \sum_{t'=0}^{t-1} \frac{\alpha^{(t')} - \bar{\mu}^2 \alpha^{(t'+1)}}{2} \|\mathbf{h}^{(t'+1)} - \mathbf{h}^{(t')}\|_2^2 + \frac{\alpha^{(t)}}{2} \|\mathbf{h}^{(t+1)} - \mathbf{h}^{(t)}\|_2^2 \\
&\geq \sum_{t'=0}^t \frac{\alpha^{(t')} - \bar{\mu}^2 \alpha^{(t'+1)}}{2} \|\mathbf{h}^{(t'+1)} - \mathbf{h}^{(t')}\|_2^2 \geq \frac{C_h \theta}{2} \sum_{t'=0}^t \|\mathbf{h}^{(t'+1)} - \mathbf{h}^{(t')}\|_2^2. \quad (79)
\end{aligned}$$

$$\begin{aligned}
f(\mathbf{x}^{(0)}, \mathbf{h}^{(0)}) - f(\mathbf{x}^{(t+1)}, \mathbf{h}^{(t+1)}) &\geq \frac{C_h \theta}{2} \sum_{t'=0}^t \|\mathbf{h}^{(t'+1)} - \mathbf{h}^{(t')}\|_2^2 - \sqrt{2\alpha^{(t')}\varepsilon^{(t')}} \|\mathbf{h}^{(t'+1)} - \mathbf{h}^{(t')}\|_2 + \frac{C_s \theta}{2} \sum_{t'=0}^t \|\mathbf{x}^{(t+1)} - \mathbf{x}^{(t')}\|_2^2 - \varepsilon^{(t')} \\
&= \frac{C_h \theta}{2} \sum_{t'=0}^t \underbrace{\left(\|\mathbf{h}^{(t'+1)} - \mathbf{h}^{(t')}\|_2 - \sqrt{2\alpha^{(t')}\varepsilon^{(t')}/(C_h \theta)} \right)^2}_{\text{denote as } h_{t'+1}^2} + \frac{C_s \theta}{2} \sum_{t'=0}^t \|\mathbf{x}^{(t+1)} - \mathbf{x}^{(t')}\|_2^2 - \underbrace{\sum_{t'=0}^t \left(1 + \frac{1}{C_h \theta} \right) \varepsilon^{(t')}}_{\text{denote as } C_\varepsilon}. \quad (81)
\end{aligned}$$

C. Convergence Speed Towards ε -Stationary Point

Adding the results in (73) and (77) from 0 to t , we get

$$\begin{aligned}
f(\mathbf{x}^{(0)}, \mathbf{h}^{(0)}) - f^* &\geq f(\mathbf{x}^{(0)}, \mathbf{h}^{(0)}) - f(\mathbf{x}^{(t+1)}, \mathbf{h}^{(t+1)}) \\
&\geq \sum_{t'=0}^t \frac{\alpha^{(t')}}{2} \left(\|\mathbf{h}^{(t'+1)} - \mathbf{h}^{(t')}\|_2^2 - \bar{\mu}^2 \|\mathbf{h}^{(t')} - \mathbf{h}^{(t'-1)}\|_2^2 \right) \\
&\quad - \sqrt{2\alpha^{(t')}\varepsilon^{(t')}} \|\mathbf{h}^{(t'+1)} - \mathbf{h}^{(t')}\|_2 - \varepsilon^{(t')} \\
&\quad + \frac{\beta^{(t')}}{2} \left(\|\mathbf{x}^{(t+1)} - \mathbf{x}^{(t')}\|_2^2 - \bar{\iota}^2 \|\mathbf{x}^{(t')} - \mathbf{x}^{(t'-1)}\|_2^2 \right), \quad (78)
\end{aligned}$$

where $f^* > -\infty$ is the lower bound of the objective function. For the first term in (78), we have the result in (79). Similarly, we also have the result

$$\begin{aligned}
\sum_{t'=0}^t \frac{\beta^{(t')}}{2} \left(\|\mathbf{x}^{(t+1)} - \mathbf{x}^{(t')}\|_2^2 - \bar{\iota}^2 \|\mathbf{x}^{(t')} - \mathbf{x}^{(t'-1)}\|_2^2 \right) \\
\geq \frac{C_s \theta}{2} \sum_{t'=0}^t \|\mathbf{x}^{(t+1)} - \mathbf{x}^{(t')}\|_2^2. \quad (80)
\end{aligned}$$

By substituting the results in (79) and (80) into (78), after some calculations, we get the result in (81). From (81), we get

$$\begin{aligned}
f(\mathbf{x}^{(0)}, \mathbf{h}^{(0)}) - f^* + C_\varepsilon &\geq \min_{t'=0,1,\dots,t} \frac{C_h \theta t}{4} (h_{t'+1}^2 + h_{t'}^2) \\
&\quad + \frac{C_s \theta t}{4} (\|\mathbf{x}^{(t'+1)} - \mathbf{x}^{(t')}\|_2^2 + \|\mathbf{x}^{(t')} - \mathbf{x}^{(t'-1)}\|_2^2). \quad (82)
\end{aligned}$$

By using Cauchy-Schwartz inequality, we have

$$\begin{aligned}
&\sqrt{f(\mathbf{x}^{(0)}, \mathbf{h}^{(0)}) - f^* + C_\varepsilon} \\
&\geq \min_{t'=0,1,\dots,t} \frac{\sqrt{C_h \theta t}}{4} \left(h_{t'+1} + h_{t'} + \|\mathbf{x}^{(t'+1)} - \mathbf{x}^{(t')}\|_2 \right. \\
&\quad \left. + \|\mathbf{x}^{(t')} - \mathbf{x}^{(t'-1)}\|_2 \right), \quad (83)
\end{aligned}$$

where $C_{h,s} = \min\{C_h, C_s\}$. For the term $\sqrt{t}h_{t'+1}$, since we require the sequence $\{\varepsilon^{(t)}\}_{t \geq 0}$ to be summable and decreasing, there exists a constant number \bar{E} to be such that

$$\sqrt{t} \min_{t'=0,1,\dots,t} \sqrt{2\alpha^{(t')}\varepsilon^{(t')}} \leq \sqrt{2t\bar{\alpha}\varepsilon^{(t)}} \leq \bar{E} < \infty, \forall t. \quad (84)$$

Therefore, combine the results in (69), (83), and (84) together, we finally get

$$\text{dist}(\mathbf{0}, \partial_{\varepsilon^{(t)}} F(\mathbf{x}^{(t+1)}, \mathbf{h}^{(t+1)})) \leq \frac{C}{\sqrt{t}}, \quad (85)$$

where

$$C = 4\bar{C} \sqrt{\frac{f(\mathbf{x}^{(0)}, \mathbf{h}^{(0)}) - f^* + C_\varepsilon}{C_{h,s} \theta}} + \left(1 + \frac{2}{C_{h,s} \theta} \right) \bar{E}. \quad (86)$$

REFERENCES

- [1] S. Lu, F. Liu, Y. Li, K. Zhang, H. Huang, J. Zou, X. Li, Y. Dong, F. Dong, J. Zhu *et al.*, “Integrated sensing and communications: Recent advances and ten open challenges,” *IEEE Internet Things J.*, 2024.
- [2] S. Lu, F. Liu, F. Dong, Y. Xiong, J. Xu, Y.-F. Liu, and S. Jin, “Random ISAC signals deserve dedicated precoding,” *IEEE Trans. Signal Process.*, vol. 72, pp. 3453–3469, 2024.
- [3] S. Lu, F. Liu, Y. Xiong, Z. Du, Y. Cui, S. Li, W. Yuan, J. Yang, and S. Jin, “Sensing with random communication signals,” *IEEE Network*, pp. 1–1, 2025.
- [4] R. Hadani, S. Rakib, M. Tsatsanis, A. Monk, A. J. Goldsmith, A. F. Molisch, and R. Calderbank, “Orthogonal time frequency space modulation,” *2017 IEEE Wirel. Commun. Netw. Conf.*, pp. 1–13, 2017.
- [5] L. Gaudio, G. Colavolpe, and G. Caire, “OTFS vs. OFDM in the presence of sparsity: A fair comparison,” *IEEE Trans. Wirel. Commun.*, vol. 21, no. 6, pp. 4410–4423, 2022.
- [6] P. Raviteja, K. T. Phan, and Y. Hong, “Embedded pilot-aided channel estimation for OTFS in delay-Doppler channels,” *IEEE Trans. Veh. Technol.*, vol. 68, no. 5, pp. 4906–4917, may 2019.
- [7] K. Zhang, Z. Li, W. Yuan, Y. Cai, and F. Gao, “Radar sensing via OTFS signaling,” *China Commun.*, vol. 20, no. 9, pp. 34–45, 2023.
- [8] S. K. Mohammed, R. Hadani, A. Chockalingam, and R. Calderbank, “OTFS—Predictability in the delay-Doppler domain and its value to communication and radar sensing,” *IEEE BITS Inf. Theory Mag.*, vol. 3, no. 2, pp. 7–31, 2023.
- [9] P. Raviteja, K. T. Phan, Y. Hong, and E. Viterbo, “Interference cancellation and iterative detection for orthogonal time frequency space modulation,” *IEEE Trans. Wirel. Commun.*, vol. 17, no. 10, pp. 6501–6515, 2018.
- [10] N. Mehrotra, S. R. Mattu, and R. Calderbank, “Pulse shaping filter design for integrated sensing & communication with Zak-OTFS,” *arXiv preprint arXiv:2510.15195*, 2025.
- [11] P. Raviteja, K. T. Phan, and Y. Hong, “Embedded pilot-aided channel estimation for OTFS in delay-Doppler channels,” *IEEE Trans. Veh. Technol.*, vol. 68, no. 5, pp. 4906–4917, may 2019.
- [12] N. Hashimoto, N. Osawa, K. Yamazaki, and S. Ibi, “Channel estimation and equalization for CP-OFDM-based OTFS in fractional Doppler channels,” in *2021 IEEE Int. Conf. Commun. (ICC Workshops)*, 2021, pp. 1–7.

- [13] X. Wang, W. Shen, C. Xing, J. An, and L. Hanzo, "Joint bayesian channel estimation and data detection for ofts systems in leo satellite communications," *IEEE Trans. Commun.*, vol. 70, no. 7, pp. 4386–4399, 2022.
- [14] Z. Wei, W. Yuan, S. Li, J. Yuan, and D. W. K. Ng, "Off-grid channel estimation with sparse Bayesian learning for OTFS systems," *IEEE Trans. Wirel. Commun.*, vol. 21, no. 9, pp. 7407–7426, sep 2022.
- [15] Y. Shan, F. Wang, Y. Hao, J. Yuan, J. Hua, and Y. Xin, "Off-grid channel estimation using grid evolution for OTFS systems," *IEEE Trans. Wirel. Commun.*, vol. 23, no. 8, pp. 9549–9565, 2024.
- [16] Y. Wu, C. Han, and Z. Chen, "DFT-spread orthogonal time frequency space system with superimposed pilots for terahertz integrated sensing and communication," *IEEE Trans. Wirel. Commun.*, vol. 22, no. 11, pp. 7361–7376, 2023.
- [17] S. Gopalam, H. Inaltekin, I. B. Collings, and S. V. Hanly, "Optimal Zak-OTFS receiver and its relation to the radar matched filter," *IEEE Open J. Commun. Soc.*, vol. 5, pp. 4462–4482, 2024.
- [18] S. Gopalam, I. B. Collings, S. V. Hanly, H. Inaltekin, S. R. B. Pillai, and P. Whiting, "Zak-OTFS implementation via time and frequency windowing," *IEEE Trans. Commun.*, vol. 72, no. 7, pp. 3873–3889, 2024.
- [19] K. Zhang, H. Hu, and S. Lu, "Practical implementation of Zak-OTFS and its relation with OFDM," in *2025 IEEE/CIC Int. Conf. Commun. China (ICCC Workshops)*, 2025, pp. 1–6.
- [20] J. J. Benedetto, I. Konstantinidis, and M. Rangaswamy, "Phase-coded waveforms and their design," *IEEE Signal Process. Mag.*, vol. 26, no. 1, pp. 22–31, 2009.
- [21] Y. Chi and M. Ferreira Da Costa, "Harnessing sparsity over the continuum: Atomic norm minimization for superresolution," *IEEE Signal Process. Mag.*, vol. 37, no. 2, pp. 39–57, mar 2020.
- [22] M. Shao, Q. Li, W. K. Ma, and A. M. C. So, "A framework for one-bit and constant-envelope precoding over multiuser massive MISO channels," *IEEE Trans. Signal Process.*, vol. 67, no. 20, pp. 5309–5324, 2019.
- [23] Z. Wu, Y. F. Liu, W. K. Chen, and C. Masouros, "Quantized constant-envelope waveform design for massive MIMO DFRC systems," *IEEE J. Sel. Areas Commun.*, p. 1, 2025.
- [24] Z. Wu, Y.-F. Liu, B. Jiang, and Y.-H. Dai, "Efficient quantized constant envelope precoding for multiuser downlink massive mimo systems," in *Proc. IEEE Int. Conf. Acoust., Speech Signal Process. (ICASSP)*. IEEE, June 2023, pp. 1–5.
- [25] R. Li and D. Cabric, "A coordinate descent approach to atomic norm denoising," *IEEE Trans. Signal Process.*, vol. 72, pp. 5077–5090, 2024.
- [26] B. N. Bhaskar, G. Tang, and B. Recht, "Atomic norm denoising with applications to line spectral estimation," *IEEE Trans. Signal Process.*, vol. 61, no. 23, pp. 5987–5999, 2013.
- [27] B. Maramandipoor, D. Ramasamy, and U. Madhow, "Newtonized orthogonal matching pursuit: Frequency estimation over the continuum," *IEEE Trans. Signal Process.*, vol. 64, no. 19, pp. 5066–5081, 2016.
- [28] D. Bertsekas, *Nonlinear Programming*. Athena Scientific, 2016, vol. 4.
- [29] S. Li, J. Yuan, W. Yuan, Z. Wei, B. Bai, and D. W. K. Ng, "Performance analysis of coded OTFS systems over high-mobility channels," *IEEE Trans. Wirel. Commun.*, vol. 20, no. 9, pp. 6033–6048, 2021.
- [30] H. W. Kuhn, "The hungarian method for the assignment problem," *Naval research logistics quarterly*, vol. 2, no. 1-2, pp. 83–97, 1955.
- [31] M. Schmidt, N. Roux, and F. Bach, "Convergence rates of inexact proximal-gradient methods for convex optimization," in *Annu. Conf. Neural Inf. Process. Syst. 2011, NIPS 2011*, vol. 24. Curran Associates, Inc., 2011.
- [32] D. Bertsekas and A. Nedic, *Convex analysis and optimization*. Athena Scientific, 2003, vol. 1.
- [33] Y. Xu and W. Yin, "A block coordinate descent method for regularized multiconvex optimization with applications to nonnegative tensor factorization and completion," *SIAM J. Imaging Sci.*, vol. 6, no. 3, pp. 1758–1789, 2013.